6-1999

The Lagrangian spectral relaxation model for differential diffusion in homogeneous turbulence

Rodney O. Fox
Iowa State University, rofox@iastate.edu

The Lagrangian spectral relaxation model for differential diffusion in homogeneous turbulence

Abstract

The Lagrangian spectral relaxation ~LSR! model is extended to treat turbulent mixing of two passive scalars (fa and fb) with different molecular diffusivity coefficients ~i.e., differential-diffusion effects!. Because of the multiscale description employed in the LSR model, the scale dependence of differential-diffusion effects is described explicitly, including the generation of scalar decorrelation at small scales and its backscatter to large scales. The model is validated against DNS data for differential diffusion of Gaussian scalars in forced, isotropic turbulence at four values of the turbulence Reynolds number (Rl538, 90, 160, and 230! with and without uniform mean scalar gradients. The explicit Reynolds and Schmidt number dependencies of the model parameters allows for the determination of the Re ~integral-scale Reynolds number! and Sc ~Schmidt number! scaling of the scalar difference z5fa2fb . For example, its variance is shown to scale like ^z2& ;Re20.3. The rate of backscatter (bD) from the diffusive scales towards the large scales is found to be the key parameter in the model. In particular, it is shown that bD must be an increasing function of the Schmidt number for Sc<1 in order to predict the correct scalar-to-mechanical time-scale>ratios, and the correct long-time scalar decorrelation rate in the absence of uniform mean scalar gradients.

Disciplines

Catalysis and Reaction Engineering | Chemical Engineering

Comments

This article is from *Physics of Fluids*11(1999): 1550-1571, doi:10.1063/1.870018 . Posted with permission.

The Lagrangian spectral relaxation model for differential diffusion in homogeneous turbulence

R. O. Fox

Citation: Physics of Fluids (1994-present) **11**, 1550 (1999); doi: 10.1063/1.870018
View online: http://dx.doi.org/10.1063/1.870018
View Table of Contents: http://scitation.aip.org/content/aip/journal/pof2/11/6?ver=pdfcov
Published by the AIP Publishing

The Lagrangian spectral relaxation model for differential diffusion in homogeneous turbulence

R. O. Fox
Department of Chemical Engineering, Iowa State University, Ames, Iowa 50011-2230

(Received 12 June 1998; accepted 17 February 1999)

The Lagrangian spectral relaxation (LSR) model is extended to treat turbulent mixing of two passive scalars (ϕ_α and ϕ_β) with different molecular diffusivity coefficients (i.e., differential-diffusion effects). Because of the multiscale description employed in the LSR model, the scale dependence of differential-diffusion effects is described explicitly, including the generation of scalar decorrelation at small scales and its backscatter to large scales. The model is validated against DNS data for differential diffusion of Gaussian scalars in forced, isotropic turbulence at four values of the turbulence Reynolds number ($R_\lambda = 38$, 90, 160, and 230) with and without uniform mean scalar gradients. The explicit Reynolds and Schmidt number dependencies of the model parameters allows for the determination of the Re (integral-scale Reynolds number) and Sc (Schmidt number) scaling of the scalar difference $z = \phi_\alpha - \phi_\beta$. For example, its variance is shown to scale like $\langle z^2 \rangle \sim \mathrm{Re}^{-0.3}$. The rate of backscatter (β_D) from the diffusive scales towards the large scales is found to be the key parameter in the model. In particular, it is shown that β_D must be an increasing function of the Schmidt number for $\mathrm{Sc} \leqslant 1$ in order to predict the correct scalar-to-mechanical time-scale ratios, and the correct long-time scalar decorrelation rate in the absence of uniform mean scalar gradients. © *1999 American Institute of Physics.* [S1070-6631(99)01706-7]

I. INTRODUCTION

Most models for scalar mixing in turbulent flows ignore molecular-scale effects based on the assumption that at high Reynolds numbers the large scales which dominate the mixing process will be independent of the small scales, where molecular effects are most pronounced. However, it is now widely recognized[1–3] that this assumption may lead to prediction errors in models for chemically reacting flows. For example, in combustion applications, reactants with widely different molecular diffusivities (i.e., differential-diffusion effects) can lead to reduced combustion efficiency and an increased formation of certain pollutants. These observations have motivated several recent experimental[4–6] and direct numerical simulation (DNS)[7–15] studies to better understand the physics of differential diffusion and to suggest improved models for practical applications.

The inclusion of differential-diffusion effects in existing models for turbulent scalar mixing is challenging due to the multi-scale nature of the underlying physics. Models that neglect molecular-scale phenomena typically assume that the dynamics of scalar transport are dominated by the cascade of spectral energy from the large (slow) scales to small scales. The small scales are thus assumed to be in dynamic equilibrium with the large scales, thereby obviating the need for a detailed model of inter-scale energy transfer. Differential-diffusion effects, however, originate at the smallest scales in the flow before manifesting themselves at large scales due to reverse transport or backscatter.[7,11]

As shown by Yeung and Pope,[7] a detailed model of differential-diffusion effects will require an explicit representation of inter-scale scalar transport. The linear-eddy model (LEM)[16] is an example of such a model, and it has been applied to study the scaling properties of differential diffusion with respect to the Reynolds and Schmidt numbers.[17] Scalar spectral transport models are another option;[18] however, the computational requirements of such models are generally considered to be too large to be useful for practical applications. Modifications of existing ''equilibrium'' mixing models—like the conditional moment closure (CMC)[12,13] — have thus received particular attention in the recent literature.[15,14] Nevertheless, because they contain no explicit small-scale information, the closures developed for equilibrium mixing models must be supplemented with Reynolds-number-dependent terms based on classical scaling arguments.[12] Moreover, because they are based on moment closures as opposed to a full probability density function (pdf) description,[3,19] the proposed closures must either neglect the possible dependencies on chemical reactions, or make use of *ad hoc* approximations of limited generality.

Our goal in the present study is to develop a full pdf model for differential diffusion by extending the recently-proposed Lagrangian spectral relaxation (LSR) model.[20] Unlike scalar spectral transport models (e.g., EDQNM), full pdf methods have the potential of treating reacting scalars with arbitrarily complex chemistry. However, despite the importance of differential-diffusion effects in reacting flow applications, none of the available molecular mixing models for full pdf applications can account for differential diffusion. The LSR model developed in this work thus offers a computationally tractable spectral description that can be combined with full pdf models to treat complex chemically reacting flows.

The LSR model, and its predecessor the spectral relax-

ation (SR) model,[21] were introduced to improve the description of turbulent mixing of a single passive scalar. (The relationship between the SR model and the scalar spectral transport equation is explored in the Appendix.) These models explicitly account for the relaxation of a nonequilibrium scalar spectrum to its final self-similar form using a computationally-efficient multi-scale description of the flow. The latter allows for a natural extension to handle differential diffusion of a pair of passive scalars transported by the flow. In particular, the effects of backscatter on the Reynolds-number scaling of differential-diffusion effects are treated in a manner that is computationally much simpler than in a scalar spectral transport model. However, the extension of the LSR model to handle multiple scalars requires us to introduce the joint scalar dissipation rate [defined by Eq. (6)] and a multi-scale description of the scalar covariance. In Sec. II we review the Reynolds-averaged transport equations for these quantities for passive scalars.

The LSR model requires[20] a consistent molecular mixing model in order to complete the full pdf description. For multiple, correlated scalars, the formulation of such a model is nontrivial.[22,23,19] In Sec. IV, we propose a new model based on the Fokker–Planck equation[24] which requires as input the conditional scalar Laplacians and the conditional (joint) scalar dissipation rates conditioned on the values of the scalars. Examples of the conditional scalar Laplacians found from DNS studies of bounded scalars[10] demonstrate that the scalar dependence can be highly nonlinear and, hence, difficult to model in general. However, for Gaussian scalar fields, the conditional scalar Laplacians are linear[15] and the conditional (joint) scalar dissipation rates are independent of the scalars.

As a first step towards a full Lagrangian pdf model of differential diffusion, we limit our consideration in this study to Gaussian scalar fields for which considerable DNS data has been reported in the literature.[7,25,8,9,11,15] As with other flow phenomena dominated by small-scale dynamics, the availability of DNS data allows us to make detailed comparisons with difficult-to-measure quantities (such as the scalar gradient correlation function and the ''banded'' coherency spectrum) that are particularly important for understanding the scale dynamics of differential-diffusion effects. In Sec. VI, LSR model predictions for differential diffusion are compared to available DNS data for passive scalar mixing in homogeneous, isotropic, stationary turbulence. Despite the limitations of the discrete spectral description, the LSR model is able to reproduce the observed dependence of several important measures of differential diffusion as a function of the Reynolds and Schmidt numbers.

II. THEORETICAL BACKGROUND

Turbulent mixing of a passive scalar ϕ_α can be described by the Reynolds-averaged moment equations for the scalar mean and its variance. For a homogeneous scalar field with a uniform mean scalar gradient and a molecular diffusion coefficient Γ_α, the governing equations become, respectively,

$$\frac{\partial\langle\phi_\alpha\rangle}{\partial t}+\langle U_i\rangle\frac{\partial\langle\phi_\alpha\rangle}{\partial x_i}=\frac{D\langle\phi_\alpha\rangle}{Dt}=0 \tag{1}$$

and

$$\frac{D\langle\phi_\alpha'^2\rangle}{Dt}=2S_\alpha-2\langle\epsilon_\alpha\rangle, \tag{2}$$

where the mean scalar dissipation rate is defined by

$$\langle\epsilon_\alpha\rangle=\left\langle\Gamma_\alpha\frac{\partial\phi_\alpha'}{\partial x_i}\frac{\partial\phi_\alpha'}{\partial x_i}\right\rangle \tag{3}$$

(summation is implied for Roman, but not Greek indices), the scalar variance source term by

$$S_\alpha=-\langle u_i\phi_\alpha'\rangle\frac{\partial\langle\phi_\alpha\rangle}{\partial x_i}, \tag{4}$$

and $u_i=U_i-\langle U_i\rangle$, $\phi_\alpha'=\phi_\alpha-\langle\phi_\alpha\rangle$ are the fluctuation fields. Note that both the scalar dissipation rate and the scalar variance source term are unclosed.

For differential diffusion, one is also interested in the covariance between ϕ_α and a second scalar ϕ_β with molecular diffusion coefficient Γ_β for the case where $\Gamma_\alpha\neq\Gamma_\beta$. Under the same conditions as above, the governing equation for the scalar covariance can be expressed as

$$\frac{D\langle\phi_\alpha'\phi_\beta'\rangle}{Dt}=2S_{\alpha\beta}-2\delta_{\alpha\beta}\langle\epsilon_{\alpha\beta}\rangle, \tag{5}$$

where the joint scalar dissipation rate is defined by

$$\langle\epsilon_{\alpha\beta}\rangle=\left\langle\sqrt{\Gamma_\alpha\Gamma_\beta}\frac{\partial\phi_\alpha'}{\partial x_i}\frac{\partial\phi_\beta'}{\partial x_i}\right\rangle, \tag{6}$$

the scalar covariance source term by

$$S_{\alpha\beta}=-\frac{1}{2}\langle u_i\phi_\alpha'\rangle\frac{\partial\langle\phi_\beta\rangle}{\partial x_i}-\frac{1}{2}\langle u_i\phi_\beta'\rangle\frac{\partial\langle\phi_\alpha\rangle}{\partial x_i}, \tag{7}$$

and the arithmetic-to-geometric-average molecular-diffusivity ratio by

$$\delta_{\alpha\beta}=\frac{\Gamma_\alpha+\Gamma_\beta}{2\sqrt{\Gamma_\alpha\Gamma_\beta}}=\frac{1}{2}\left(\frac{\Gamma_\alpha}{\Gamma_\beta}\right)^{1/2}+\frac{1}{2}\left(\frac{\Gamma_\beta}{\Gamma_\alpha}\right)^{1/2}. \tag{8}$$

(The reason for introducing this last parameter will become obvious in Sec. V. Note, however, that it is a symmetric function of the ratio of the molecular diffusivities.) Note that unlike the scalar dissipation rate, the sign of the joint scalar dissipation rate need not be positive. For example, if the scalar fluxes are represented by a gradient-diffusion model of the form

$$\langle u_i\phi_\alpha'\rangle=-D_T\frac{\partial\langle\phi_\alpha\rangle}{\partial x_i}, \tag{9}$$

the covariance source term becomes

$$S_{\alpha\beta}=D_T\frac{\partial\langle\phi_\alpha\rangle}{\partial x_i}\frac{\partial\langle\phi_\beta\rangle}{\partial x_i}. \tag{10}$$

Thus, its sign depends on the relative alignment of the mean scalar gradients. If these gradients are colinear, but point in opposite directions, the covariance source term will be nega-

tive, thereby forcing the joint scalar dissipation rate to be negative. Moreover, if the gradient directions were suddenly switched so that the covariance source term is positive, the joint scalar dissipation rate would smoothly evolve from negative to positive values. This type of dynamical behavior should be accounted for in a completely general model for differential diffusion.

Two widely-used measures of differential diffusion are the correlation coefficient for the scalars:

$$\rho_{\alpha\beta}=\frac{\langle \phi'_\alpha \phi'_\beta\rangle}{\sqrt{\langle \phi'^2_\alpha\rangle\langle \phi'^2_\beta\rangle}}, \tag{11}$$

and the correlation coefficient for the scalar gradients:

$$g_{\alpha\beta}=\frac{\langle \epsilon_{\alpha\beta}\rangle}{\sqrt{\langle \epsilon_\alpha\rangle\langle \epsilon_\beta\rangle}}. \tag{12}$$

The first of these is dominated by the energy-containing scales of the scalar field (i.e., scales near the velocity-integral scale). At high Reynolds numbers, the large scales are not directly affected by molecular diffusion. Thus, two initially perfectly-correlated scalar field $[\rho_{\alpha\beta}(0)=1]$ will slowly decorrelate due to differential-diffusion effects that begin in the diffusive scales and **backscatter** to the large scales.

The gradient correlation coefficient, on the other hand, is dominated by the diffusive scales and thus quickly responds to differential diffusion. Due to its small-scale nature, $g_{\alpha\beta}$ is extremely difficult to measure experimentally, but can easily be extracted from DNS data. Nevertheless, the gradient correlation coefficient plays a key role[7] in determining the long-time behavior of $\rho_{\alpha\beta}$ in the absence of mean scalar gradients, and thus must be accurately modeled when accounting for differential diffusion. As we shall see in Sec. V, the multi-scale description employed in the LSR model makes it particularly well suited for describing the scale-specific behavior of the correlation coefficients with minimal computational effort. Note that in the special case where the mean scalar gradients are colinear and the scalar fluxes can be represented by the gradient-diffusion model, the steady-state gradient correlation coefficient obeys

$$g_{\alpha\beta}=\frac{1}{\delta_{\alpha\beta}}. \tag{13}$$

This behavior has been observed in DNS studies[15] and should be reproduced by a general model for differential diffusion.

From the discussion above, it should be clear that the key unclosed quantities needed to describe differential-diffusion effects for homogeneous passive scalar mixing are the scalar dissipation rates $\langle \epsilon_\alpha\rangle$ and the joint scalar dissipation rate $\langle \epsilon_{\alpha\beta}\rangle$. The SR model provides a multi-scale closure for the scalar dissipation rate with explicit dependence on the turbulence Reynolds number:

$$\mathrm{Re}_1=\frac{\langle k\rangle}{\sqrt{\nu\langle \epsilon\rangle}}=0.3873R_\lambda, \tag{14}$$

and the Schmidt number:

$$\mathrm{Sc}_\alpha=\frac{\nu}{\Gamma_\alpha}, \tag{15}$$

where $\langle k\rangle$ is the mean turbulent kinetic energy, $\langle \epsilon\rangle$ is the mean turbulent dissipation rate, and ν is the kinematic viscosity. The relationship between the SR model and the fundamental scalar spectrum evolution equations is discussed in detail in the Appendix. The SR model has been extended[20] to model the coupling between the scalar dissipation rate and small-scale velocity fluctuations for a Lagrangian fluid particle (i.e., the LSR model).

In this work, the LSR model is extended to include a multi-scale closure for the joint scalar dissipation rate $\langle \epsilon_{\alpha\beta}\rangle$. As shown in Sec. IV, the model equation for the joint scalar dissipation rate is nearly identical to that for the scalar dissipation rate. Thus, the key new features that are required to model successfully differential diffusion are (1) the inclusion of backscatter from small to large scales, and (2) a molecular mixing model to describe the evolution of the joint scalar PDF. (See the Appendix for an exact definition of backscatter in terms of scalar-variance transfer spectrum.)

In Sec. V, LSR model predictions are compared to DNS data for differential diffusion of two scalars with Schmidt numbers in the range $1/8\leqslant \mathrm{Sc}_\alpha\leqslant 1$ for Taylor-scale Reynolds numbers in the range $38\leqslant R_\lambda\leqslant 230$. The original LSR model was formulated for $1<\mathrm{Sc}_\alpha$, thus in Sec. III the model equations for $\mathrm{Sc}_\alpha\leqslant 1$ are discussed, backscatter terms are added, and minor revisions to the original model are introduced. Further details on the choice of model parameters and on the Lagrangian pdf description can be found in the literature.[21,20] In Sec. IV, the extension of the model to treat differential diffusion is presented. As noted in our previous work,[20] the complete Lagrangian pdf model includes a Lagrangian model for the fluctuating velocity, obviating the need for a scalar flux model such as the gradient-diffusion model given in Eq. (9). However, for the Gaussian scalar fields in isotropic turbulence considered in this work, use of the gradient-diffusion model has no influence on the model predictions for differential diffusion, and thus we employ a stochastic gradient-diffusion model for the scalar flux which is described in Sec. IV.

III. SPECTRAL RELAXATION MODEL FOR THE SCALAR DISSIPATION RATE

A. Overview of the SR model

The most general form of the spectral relaxation model[20] describes the scalar dissipation rate following a Lagrangian fluid particle [i.e., a random time-dependent function $\langle \epsilon_\phi\rangle^*(t)$ where the * denotes the conditional expected value]. In homogeneous systems, averaging over all fluid particles leads to an Eulerian model for the mean scalar dissipation rate $\langle \epsilon_\phi\rangle$ referred to as the SR model. The SR model describes the nonequilibrium transport of scalar energy as a cascade process from large to small scales. The spectral transport is assumed to be local in scalar wavenumber space,[25,11] and the velocity spectrum is assumed to be fully

developed (i.e., equilibrium turbulence). The SR model variables are the fraction of the scalar spectrum, $E_\phi(\kappa,t)$, in finite wavenumber bands $[\kappa_{i\,j-1},\kappa_{ij})$:

$$\langle \phi'^2\rangle_{ij}=\int_{\kappa_{ij-1}}^{\kappa_{ij}} E_\phi(\kappa,t)d\kappa. \tag{16}$$

(In this section, we will drop the Greek subscript indicating a particular scalar field.) The scalar variance can then be found by summing over all wavenumber bands. Likewise, the fraction of the scalar energy in a particular wavenumber band is given by

$$\langle \mathfrak{s}\rangle_{ij}=\frac{\langle \phi'^2\rangle_{ij}}{\langle \phi'^2\rangle}. \tag{17}$$

Note that by definition $0\leqslant\langle \mathfrak{s}\rangle_{ij}\leqslant 1$ and the sum of all fractions is unity.

In order to keep the model computationally tractable, the wavenumbers κ_{ij} are chosen to *minimize the number of substages* required to model a flow with given Reynolds and Schmidt numbers. For $\mathrm{Sc}\leqslant 1$, the principal wavenumbers that appear in the model are as follows.

(1) The Kolmogorov-scale wavenumber:
$$\kappa_\eta=\left(\frac{\langle\epsilon\rangle}{\nu^3}\right)^{1/4}. \tag{18}$$
(2) The velocity-dissipation wavenumber: $\kappa_U=C_U^{3/2}\kappa_\eta$.
(3) The scalar-dissipation wavenumber: $\kappa_D=C_D^{1/2}\,\mathrm{Sc}^{1/2}\,\kappa_\eta$.
(4) The inertial-subrange wavenumbers $(1\leqslant j<n_2)$:
$$\kappa_{2j}=\left(\frac{3^j}{C_U\,\mathrm{Re}_1+3^j-1}\right)^{3/2}\kappa_U, \tag{19}$$
where the number of substages n_2 is an increasing function of $\ln(\mathrm{Re}_1)$.
(5) The integral-scale wavenumber: $\kappa_0=\mathrm{Re}_1^{-3/2}\,\kappa_\eta$.

The wavenumber bands are thus completely determined by the two model constants C_D and C_U.

In theory, C_U should be chosen such that κ_U lies at the boundary between the inertial and dissipative subranges of the velocity spectrum. Likewise, κ_D should lie at the boundary between the inertial-convective and the inertial-diffusive subranges of the scalar spectrum. In the SR model, in order to have the correct balance between the scalar energy flux to dissipative scales and molecular dissipation, C_D is fixed at $C_D=C_s/(C_d-1)=1/4$. (C_s and C_d are defined below. See the Appendix for exact definitions in terms of the scalar spectrum.) Note that this choice results in $\kappa_D=\kappa_\eta/2$ for a unity-Schmidt-number scalar. In this work, we will consider only Schmidt numbers large enough so that $\kappa_{2\,n_2-1}\leqslant\kappa_D$. The minimum Schmidt numbers which satisfy this condition, as functions of selected R_λ and n_2, are given in Table I. Nevertheless, by employing a smaller number of substages when the Schmidt number is less than the minimum value, it would be possible to extend the model to handle scalars with smaller Schmidt numbers.

As noted above, C_U determines the start of the velocity-dissipation scales. One way to fix C_U (given C_D) is to force $\kappa_U=\kappa_D$ for a particular value of the Schmidt number Sc*:

TABLE I. Applicable ranges for R_λ and Sc for fixed values of the number of inertial range substages n_2. Note that the minimum Schmidt number decreases with increasing Reynolds number for fixed n_2.

n_2	2	3	4
Minimum R_λ	20	60	180
Minimum Sc	0.341	0.293	0.279
Maximum R_λ	60	180	750
Minimum Sc	0.063	0.058	0.029

$$C_U=(C_D\,\mathrm{Sc}^*)^{1/3}. \tag{20}$$

In this work, we shall choose $\mathrm{Sc}^*=1$ which yields $C_U=0.63$ and $\kappa_U=\kappa_D/2$. However, one could also choose, for example, Sc* to be the Schmidt number for which the velocity and scalar dissipation spectra peak at the same wavenumber. DNS data ($R_\lambda=38$) indicate that this occurs at approximately $\mathrm{Sc}^*=1/4$.[26] This choice yields $\kappa_U=\kappa_\eta/4$ and reflects the fact that the scalar energy spectrum for a unity-Schmidt-number scalar extends to higher wavenumbers than does the velocity spectrum. Alternatively, experimental/DNS data suggest that $\kappa_U\approx 0.1\kappa_\eta$ which yields $C_U\approx 0.22$. Simulation results for differential diffusion were found to be insensitive to the choice of C_U in the range [0.22, 0.63].

For the range of Reynolds numbers used in DNS studies of differential diffusion[15] ($R_\lambda\leqslant 230$), the minimum number of inertial-range substages needed for the SR model is $2\leqslant n_2\leqslant 4$ (see Table I). For example, with $n_2=3$, the scalar spectrum is split into five substages for which the model variables and wavenumber bands are as follows.

- $\langle \phi'^2\rangle_1$ for wavenumbers $0\leqslant\kappa\leqslant\kappa_0$,
- $\langle \phi'^2\rangle_{21}$ for wavenumbers $\kappa_0<\kappa\leqslant\kappa_{21}$,
- $\langle \phi'^2\rangle_{22}$ for wavenumbers $\kappa_{21}<\kappa\leqslant\kappa_{22}$,
- $\langle \phi'^2\rangle_{23}$ for wavenumbers $\kappa_{22}<\kappa\leqslant\kappa_D$,
- $\langle \phi'^2\rangle_D$ for wavenumbers $\kappa_D<\kappa$.

The model equations[20] for the substage scalar variances are linear in the model variables $\langle \phi'^2\rangle_{ij}$, and contain a source term due to the mean scalar gradient that is proportional to the scalar-variance source term S_{ϕ^2}. All scalar dissipation is assumed to occur at wavenumbers greater than κ_D so that the scalar variance in the dissipative subrange is governed by

$$\frac{D\langle \phi'^2\rangle_D}{Dt}=2T_D+2\gamma_D S_{\phi^2}-2\langle\epsilon_\phi\rangle, \tag{21}$$

where T_D models the spectral transport of scalar energy into the dissipative range, $\gamma_D=1/(C_D\,\mathrm{Re}_1)$ is the fraction of the scalar-variance source term that falls in the dissipative range, and $\langle\epsilon_\phi\rangle$ is the mean scalar dissipation rate. [See the Appendix for the exact definition of the terms on the right-hand side of Eq. (21) derived from the scalar spectrum and scalar transfer spectrum.]

B. Specification of the spectral transport rate constants

In previous applications of the SR model,[21,20] spectral transport of scalar energy was assumed to occur only from large to small scales (i.e., a forward cascade). However, in

order to describe differential-diffusion effects, it is essential that *backscatter* from small to large scales be included. Because the SR model is linear in the substage scalar variances, spectral transport can be represented schematically in terms of forward (α) and backscatter (β) transport rates:

$$\langle \phi'^2\rangle_1 \underset{\beta_{21}}{\overset{\alpha_1}{\rightleftharpoons}} \langle \phi'^2\rangle_{21} \underset{\beta_{22}}{\overset{\alpha_{21}}{\rightleftharpoons}} \langle \phi'^2\rangle_{22} \underset{\beta_{23}}{\overset{\alpha_{22}}{\rightleftharpoons}} \langle \phi'^2\rangle_{23} \underset{\beta_D}{\overset{\alpha_{23}}{\rightleftharpoons}} \langle \phi'^2\rangle_D .$$

(See the Appendix for the exact definition of the rate constants in terms of the scalar-variance transfer spectrum.) As we shall see in Sec. IV, due to linearity, the extension of the model to describe the scalar covariance is straight forward, and simply requires the replacement of the substage scalar variances with the substage scalar covariances. In terms of the forward and backscatter rate constants, the spectral transport term in Eq. (21) is given by

$$T_D = \alpha_{23}\langle \phi'^2\rangle_{23} - \beta_D \langle \phi'^2\rangle_D . \tag{22}$$

In previous applications of the model,[21,20] the forward rate constants were defined in terms of characteristic time scales t_{ij} for each substage. The same time scales are used in the present work; however, for $\mathrm{Sc}\leqslant 1$, the time scale for the final inertial-range substage $t_{2\,n_2}$ must be modified as follows:

$$t_{2\,n_2} = \frac{1}{2}\left[t_{2\,n_2-1} - \frac{3}{C_U \mathrm{Re}_1}(\mathrm{Sc}^{-1/3}-1)t_1 \right]. \tag{23}$$

(Note that the requirement that $t_{2\,n_2}$ be positive (i.e., $\kappa_{2\,n_2-1}\leqslant \kappa_D$) puts a lower limit on the Schmidt number.) In isotropic turbulence, the characteristic time scale for the energy-containing scales t_1 is inversely proportional the turbulence frequency $\langle \omega\rangle = \langle \epsilon\rangle/\langle k\rangle$.

With the addition of backscatter, the forward rate constants are defined by

$$\alpha_{ij} = (1+c_d)t_{ij}^{-1}, \tag{24}$$

where the model parameter c_d controls the rate of backscatter from small to large scales. In Sec. V, by examining the time evolution of the scalar cospectrum, we find that $c_d = 1$ yields good agreement with DNS data. The backscatter rate constants β_{ij} are then fixed by enforcing a local ''detailed-balance'' criterion which states that the self-similar scalar spectrum for $\mathrm{Sc}=1$ must have exactly the same form regardless of the value of c_d. (Alternatively, the backscatter rates could be extracted from DNS data as discussed in the Appendix.) Applying this criterion, the backscatter rate constants become

$$\beta_{2j} = c_d(t_{2j}^{-1} - t_1^{-1}), \tag{25}$$

for $1\leqslant j\leqslant n_2$, and

$$\beta_D = c_d h(\mathrm{Sc})(C_D \mathrm{Re}_1 - 1)t_1^{-1}, \tag{26}$$

where

$$h(\mathrm{Sc}) = c_b \frac{\kappa_D}{\kappa_U} \tag{27}$$

is a function of Sc through κ_D.

The explicit Schmidt-number dependence in Eq. (26) will result in a Sc-dependent scalar dissipation rate, as is observed in DNS.[7] In Sec. V, we shall see that $c_b = 1$ yields good agreement with DNS, and that an explicit Sc dependence is required in order to predict the correct long-time, large-scale decorrelation due to differential diffusion. The functional form used in Eq. (27) has been validated using DNS data at $R_\lambda = 90$. In a detailed study (to be reported in a future communication) using DNS data at Reynolds numbers between 38 and 230, it has been found that the Schmidt number dependence of β_D shows little dependence on Reynolds number. For the SR model, the explicit Schmidt-number dependence of β_D is a necessary condition for predicting the backscatter of spectral incoherency from small to large scales.

C. Scalar dissipation rate

The remaining unclosed term is the mean scalar dissipation rate. In the SR model, it is governed by

$$\begin{aligned}\frac{D\langle \epsilon_\phi\rangle}{Dt} &= 2C_D \mathrm{Re}_1\langle \omega\rangle \alpha_{23}\langle \phi'^2\rangle_{23} - 2\beta_D\langle \epsilon_\phi\rangle \\ &\quad + 2\gamma_D S_{\phi^2}\frac{\langle \epsilon_\phi\rangle}{\langle \phi'^2\rangle_D} + 2C_s \mathrm{Re}_1\langle \omega\rangle\langle \epsilon_\phi\rangle \\ &\quad - 2C_d\frac{\langle \epsilon_\phi\rangle}{\langle \phi'^2\rangle_D}\langle \epsilon_\phi\rangle .\end{aligned} \tag{28}$$

(See the Appendix for a derivation of the key terms is this model starting from the scalar spectral transport equation.) Note that from the definition of the scalar-dissipation wavenumber,

$$C_D \mathrm{Re}_1\langle \omega\rangle = \Gamma \kappa_D^2. \tag{29}$$

Thus, the first term on the right-hand side of Eq. (28) is just the scalar energy entering the dissipation range due to forward transport multiplied by the characteristic scalar frequency at the dissipation scale. The second term is the loss of scalar dissipation due to backscatter out of the dissipation range. The third term is the contribution of the scalar-variance source term that falls in the dissipation range. (This term is negligible for large Reynolds numbers.) The fourth term is the scalar-gradient-amplification term due to small-scale vortex stretching[27] ($C_s = 1/2$). The fifth term is the molecular dissipation term[21] ($C_d = 3$) whose characteristic frequency is

$$\langle r_\phi\rangle_D = \frac{\langle \epsilon_\phi\rangle}{\langle \phi'^2\rangle_D}. \tag{30}$$

Note that because $\langle \phi'^2\rangle_D$ is inversely proportional to the turbulence Reynolds number, $\langle r_\phi\rangle_D \sim \mathrm{Re}_1$. Thus, at steady state, the production terms in Eq. (28) due to spectral transport from large scales and gradient amplification will be exactly balanced by molecular dissipation. Moreover, the time needed to reach steady state will be proportional to the Kolmogorov time scale $\tau_\eta = \mathrm{Re}_1\langle \omega\rangle$. Hence, unlike the ''small-scale equilibrium'' models (see Sanders and Gölkalp[28] for a recent review) which equate the scalar dissipation rate to the

scalar-energy flux through the inertial range, Eq. (28) represents a true small-scale model for the scalar dissipation rate. For this reason, integral-scale terms such as the mean shear rate,

$$\frac{\partial\langle U_j\rangle}{\partial x_i}, \tag{31}$$

or the mean scalar frequency,

$$\langle r_\phi\rangle = \frac{\langle\epsilon_\phi\rangle}{\langle\phi'^2\rangle}, \tag{32}$$

that appear in the small-scale equilibrium models do not appear in Eq. (28). Thus, because it describes the smallest scales in a turbulent flow, the scalar dissipation rate model used in the SR model should be universal at Reynolds numbers high enough to ensure a separation between the energy-containing and dissipative scales.

This conclusion, however, leaves open the problem of incorporating the known effects of integral-scale terms on the mean scalar dissipation rate. Although beyond the scope of the present work, it is important to note that in the SR model these effects would appear into the forward and backscatter rate constants which control the flux of scalar energy to small scales. For example, t_1, which in isotropic turbulence is set equal to the turbulent integral time scale $\langle k\rangle/\langle\epsilon\rangle$, would need to be modified to include the effect of a mean shear. Such a modification could be proposed and validated using results from DNS studies of scalar spectral energy transport in homogeneous shear flows similar to those already reported for scalar mixing in isotropic turbulence.[25,11]

D. Lagrangian pdf version

The SR model gives no information about the scalar pdf which is required, for example, to close the chemical source term for reacting flows. The Lagrangian pdf version (i.e., the LSR model) provides this information, and has a form very similar to the SR model. Details on the model formulation can be found in the literature.[20] However, the principal modification is the introduction of a fluctuating gradient-amplification term in the scalar dissipation rate model:

$$C_s\,\mathrm{Re}_1\langle\omega\rangle\langle\epsilon_\phi\rangle \to C_s\,\mathrm{Re}_1\langle\omega\rangle\sigma(t)\langle\epsilon_\phi\rangle^*, \tag{33}$$

where the random strain term is defined in terms of the Lagrangian turbulent frequency $\omega^*(t)$:[29,30]

$$\sigma(t) = \left(\frac{\omega^*}{\langle\omega\rangle}\right)^{1/2}. \tag{34}$$

Note that the only random variable which appears as an input to the LSR model is $\omega^*(t)$. The user is thus free to choose an appropriate stochastic model to mimic the Lagrangian behavior of the turbulent dissipation. In this work, we will use the stretched-exponential model proposed by Fox[20] with $\langle\omega\rangle=1$, $S_\omega=h=0$, and $C_\chi=5/\mathrm{Re}_1$ based on DNS data.[31] The constant C_χ controls the Lagrangian autocorrelation time in homogeneous turbulence. Here we use the value found by Dreeben and Pope[32] (C_χ is equivalent to C_3 in their model) to yield the correct turbulent dissipation flux in near-wall turbulent flows. As shown in our earlier work,[20] the stretched-exponential model yields good agreement with DNS data[31] for one-point, one-time statistics of the scalar dissipation rate. The model chosen for $\omega^*(t)$ will also determine the behavior of Lagrangian time series for the scalar dissipation rate. The model's agreement with DNS Lagrangian time series is still an open question; however, it is important to note that the LSR model formulation does not depend on the choice of the model for $\omega^*(t)$.

The LSR model equations are written in terms of the Lagrangian conditional expectations:[20] $\langle\phi'^2\rangle_{ij}^*$ and $\langle\epsilon_\phi\rangle^*$. For example, the characteristic frequency for molecular dissipation in the scalar dissipation rate model becomes

$$\langle r_\phi\rangle_D \to \langle r_\phi\rangle_D^\dagger = \frac{\langle\epsilon_\phi\rangle^*}{\langle\phi'^2\rangle_D^*}. \tag{35}$$

(Because $\langle\cdot\rangle\neq\langle\langle\cdot\rangle^\dagger\rangle$ where the second expected value is with respect to all fluid particles, we use a † to denote the ratio of two Lagrangian variables.) Note, however, that because each fluid particle is subject to its own strain-rate history, the Lagrangian scalar variance $\langle\phi'^2\rangle^*$ will not be equal to the Eulerian scalar variance $\langle\phi'^2\rangle$. Thus, an additional model variable,

$$\Phi = \frac{\langle\phi'^2\rangle^*}{\langle\phi'^2\rangle}, \tag{36}$$

must be introduced, as well as the Lagrangian scalar-variance fractions:

$$\langle \mathbf{s}\rangle_{ij}^\dagger = \frac{\langle\phi'^2\rangle_{ij}^*}{\langle\phi'^2\rangle^*}. \tag{37}$$

These variables will appear in the molecular mixing model for the Lagrangian scalar $\phi^*(t)$ presented in Sec. IV.

The only other modification appearing in the LSR model are terms that describe interactions between the ''local'' and ''global'' variables. These terms were added primarily to provide a simple description of spectral relaxation for inhomogeneous flows, and thus have a negligible influence on the model prediction for the homogeneous flows considered in this work. As an example, with $n_2=3$, the Lagrangian scalar dissipation rate is governed by

$$\begin{aligned}\frac{D\langle\epsilon_\phi\rangle^*}{Dt} &= 2C_D\,\mathrm{Re}_1\langle\omega\rangle\alpha_{23}(f_{23}\langle\phi'^2\rangle_{23}^* + f_{23}^c\langle\phi'^2\rangle_{23}) \\ &\quad - 2\beta_D\langle\epsilon_\phi\rangle^* + 2\gamma_D\langle r_\phi\rangle_D(\langle\epsilon_\phi\rangle - \langle\epsilon_\phi\rangle^*) \\ &\quad + 2\gamma_D S_{\phi^2}\langle r_\phi\rangle_D^\dagger + 2C_s\,\mathrm{Re}_1\langle\omega\rangle\sigma(t)\langle\epsilon_\phi\rangle^* \\ &\quad - 2C_d\langle r_\phi\rangle_D^\dagger\langle\epsilon_\phi\rangle^*\end{aligned} \tag{38}$$

(note the fluctuating strain-rate term in the next-to-last term on the right-hand side), and the Lagrangian scalar variance in the dissipation range is governed by

$$\begin{aligned}\frac{D\langle\phi'^2\rangle_D^*}{Dt} &= 2\alpha_{23}(f_{23}\langle\phi'^2\rangle_{23}^* + f_{23}^c\langle\phi'^2\rangle_{23}) - 2\beta_D\langle\phi'^2\rangle_D^* \\ &\quad + 2\gamma_D\langle r_\phi\rangle_D(\langle\phi'^2\rangle_D - \langle\phi'^2\rangle_D^*) + 2\gamma_D S_{\phi^2} \\ &\quad - 2\langle\epsilon_\phi\rangle^*,\end{aligned} \tag{39}$$

where $f_{23}=\kappa_D/\kappa_U$ and $f_{23}^c=1-f_{23}$. The first term on the right-hand side of each equation represents the forward transport from larger scales. It is split into two parts representing (1) forward transport within the same fluid particle, and (2) forward transport from other particles. The second term represents backscatter to larger scales. The third term represents exchange between particles due to molecular dissipation. The fourth term is the contribution from the scalar-variance source. The final term in Eq. (39) is the ''local'' scalar dissipation rate. The model equations for other wavenumber bands are similar to Eq. (39) and can be found in our earlier work.[20]

When studying differential-diffusion effects, the LSR model is applied to each scalar (ϕ_α and ϕ_β) separately. This is done by making the following substitutions in the model equations:

$$\mathrm{Sc}\to\mathrm{Sc}_\alpha,$$
$$S_{\phi^2}\to S_\alpha,$$
$$\langle\phi'^2\rangle_{ij}\to\langle\phi'^2_\alpha\rangle_{ij},$$
$$\langle\phi'^2\rangle^*_{ij}\to\langle\phi'^2_\alpha\rangle^*_{ij},$$
$$\langle\mathfrak{s}\rangle_{ij}\to\langle\mathfrak{s}_\alpha\rangle_{ij},$$
$$\langle\mathfrak{s}\rangle^\dagger_{ij}\to\langle\mathfrak{s}_\alpha\rangle^\dagger_{ij},$$
$$\Phi\to\Phi_\alpha,$$
$$\langle\epsilon_\phi\rangle\to\langle\epsilon_\alpha\rangle,$$
$$\langle\epsilon_\phi\rangle^*\to\langle\epsilon_\alpha\rangle^*,$$
$$\langle r_\phi\rangle_D\to\langle r_\alpha\rangle_D,$$
$$\langle r_\phi\rangle^\dagger_D\to\langle r_\alpha\rangle^\dagger_D,$$
$$\langle r_\phi\rangle\to\langle r_\alpha\rangle,$$
$$\langle r_\phi\rangle^\dagger\to\langle r_\alpha\rangle^\dagger.$$

Note that of the wavenumbers used to define the LSR model, only the scalar-dissipation wavenumber depends explicitly on the Schmidt number, i.e., $\kappa_{D\alpha}\neq\kappa_{D\beta}$ when $\mathrm{Sc}_\alpha\neq\mathrm{Sc}_\beta$. Likewise, only the backscatter rate from the dissipation range (β_D) depends on the Schmidt number. In the next section, the LSR model is extended to describe differential diffusion. In Sec. V we shall see that the Schmidt-number dependence of the backscatter rate plays a critical role in determining the long-time behavior of the correlation coefficients $\rho_{\alpha\beta}$ and $g_{\alpha\beta}$.

IV. EXTENSION TO DIFFERENTIAL DIFFUSION

A. LSR model for the joint scalar dissipation rate

The LSR model for the joint scalar dissipation rate is found by making the following substitutions in the model equations for a single scalar:

$$\mathrm{Sc}\to\mathrm{Sc}_{\alpha\beta}=\frac{2\nu}{\Gamma_\alpha+\Gamma_\beta},$$
$$t_{2\,n_2}\to\frac{1}{2}\left[t_{2\,n_2-1}-\frac{3}{C_U\,\mathrm{Re}_1}(\mathrm{Sc}_{\alpha\beta}^{-1/3}-1)t_1\right],$$
$$S_{\phi^2}\to S_{\alpha\beta},$$
$$\langle\phi'^2\rangle_{ij}\to\langle\phi'_\alpha\phi'_\beta\rangle_{ij},$$
$$\langle\phi'^2\rangle^*_{ij}\to\langle\phi'_\alpha\phi'_\beta\rangle^*_{ij},$$
$$\langle\epsilon_\phi\rangle\to\delta_{\alpha\beta}\langle\epsilon_{\alpha\beta}\rangle,$$
$$\langle\epsilon_\phi\rangle^*\to\delta_{\alpha\beta}\langle\epsilon_{\alpha\beta}\rangle^*,$$

where $\mathrm{Sc}_{\alpha\beta}$ defines the covariance-dissipation wavenumber: $\kappa_{D\alpha\beta}=C_D^{1/2}\mathrm{Sc}_{\alpha\beta}^{1/2}\kappa_\eta$.

These substitutions in Eq. (39) lead to a scalar-dissipation-range covariance equation of the form

$$\frac{D\langle\phi'_\alpha\phi'_\beta\rangle^*_D}{Dt}=2\alpha_{23}(f_{23}\langle\phi'_\alpha\phi'_\beta\rangle^*_{23}+f^c_{23}\langle\phi'_\alpha\phi'_\beta\rangle_{23})-2\beta_D\langle\phi'_\alpha\phi'_\beta\rangle^*_D+2\gamma_D\delta_{\alpha\beta}\langle r_{\alpha\beta}\rangle_D(\langle\phi'_\alpha\phi'_\beta\rangle_D-\langle\phi'_\alpha\phi'_\beta\rangle^*_D)+2\gamma_D S_{\alpha\beta}-2\delta_{\alpha\beta}\langle\epsilon_{\alpha\beta}\rangle^*, \quad (40)$$

where α_{23} is computed using the new definition for t_{23}, and the Eulerian characteristic covariance-dissipation frequency is defined by

$$\langle r_{\alpha\beta}\rangle_D=\frac{\langle\epsilon_{\alpha\beta}\rangle}{\langle\phi'_\alpha\phi'_\beta\rangle_D}. \quad (41)$$

Likewise, the model equation for the joint scalar dissipation rate becomes

$$\frac{D\langle\epsilon_{\alpha\beta}\rangle^*}{Dt}=2C_D\,\mathrm{Re}_1\langle\omega\rangle\delta_{\alpha\beta}^{-1}\alpha_{23}(f_{23}\langle\phi'_\alpha\phi'_\beta\rangle^*_{23}+f^c_{23}\langle\phi'_\alpha\phi'_\beta\rangle_{23})-2\beta_D\langle\epsilon_{\alpha\beta}\rangle^*+2\gamma_D\delta_{\alpha\beta}\langle r_{\alpha\beta}\rangle_D(\langle\epsilon_{\alpha\beta}\rangle-\langle\epsilon_{\alpha\beta}\rangle^*)+2\gamma_D S_{\alpha\beta}\langle r_{\alpha\beta}\rangle^\dagger_D+2C_s\,\mathrm{Re}_1\langle\omega\rangle\sigma(t)\langle\epsilon_{\alpha\beta}\rangle^*-2C_d\delta_{\alpha\beta}\langle r_{\alpha\beta}\rangle^\dagger_D\langle\epsilon_{\alpha\beta}\rangle^*, \quad (42)$$

where the Lagrangian characteristic covariance-dissipation frequency is defined by

$$\langle r_{\alpha\beta}\rangle^\dagger_D=\frac{\langle\epsilon_{\alpha\beta}\rangle^*}{\langle\phi'_\alpha\phi'_\beta\rangle^*_D}, \quad (43)$$

i.e., the ratio of two variables dominated by small scales.

As shown next, $\langle\phi'_\alpha\phi'_\beta\rangle_D$ and $\langle\epsilon_{\alpha\beta}\rangle$ will always have the same sign so that $\langle r_{\alpha\beta}\rangle_D$ is always positive. This would not be the case if, for example,

$$\langle r_{\alpha\beta}\rangle^\dagger=\frac{\langle\epsilon_{\alpha\beta}\rangle^*}{\langle\phi'_\alpha\phi'_\beta\rangle^*} \quad (44)$$

were used to define the characteristic covariance-dissipation frequency because the scalar covariance is dominated by large scales. In Sec. V, we shall see that this property allows us to successfully apply the model to the case where the mean scalar gradients are suddenly switched from pointing in the same direction to pointing in opposite directions. For

this example, the small scales pass from positive to negative correlation before the large scales. For this case, if Eq. (44) were used to define the characteristic frequency, the model would be unstable when the covariance approached zero.

By combining Eqs. (40) and (42), the governing equation for $\langle r_{\alpha\beta}\rangle_D^\dagger$ is found to be

$$\begin{aligned}\frac{D\langle r_{\alpha\beta}\rangle_D^\dagger}{Dt} &= 2\alpha_{23}\left(f_{23}\frac{\langle \phi'_\alpha\phi'_\beta\rangle_{23}^*}{\langle \phi'_\alpha\phi'_\beta\rangle_D^*} + f_{23}^c\frac{\langle \phi'_\alpha\phi'_\beta\rangle_{23}}{\langle \phi'_\alpha\phi'_\beta\rangle_D^*}\right)\\ &\quad\times(C_D\,\mathrm{Re}_1\langle\omega\rangle\delta_{\alpha\beta}^{-1}-\langle r_{\alpha\beta}\rangle_D^\dagger)\\ &\quad+2\gamma_D\delta_{\alpha\beta}\langle r_{\alpha\beta}\rangle_D\frac{\langle \phi'_\alpha\phi'_\beta\rangle_D}{\langle \phi'_\alpha\phi'_\beta\rangle_D^*}(\langle r_{\alpha\beta}\rangle_D\\ &\quad-\langle r_{\alpha\beta}\rangle_D^\dagger)+2C_s\,\mathrm{Re}_1\langle\omega\rangle\sigma(t)\langle r_{\alpha\beta}\rangle_D^\dagger\\ &\quad-2(C_d-1)\delta_{\alpha\beta}(\langle r_{\alpha\beta}\rangle_D^\dagger)^2. \end{aligned} \tag{45}$$

Note that the right-hand side of this expression will be null if $\sigma(t)=1$ and

$$\langle r_{\alpha\beta}\rangle_D^\dagger=\langle r_{\alpha\beta}\rangle_D=C_D\,\mathrm{Re}_1\langle\omega\rangle\delta_{\alpha\beta}^{-1}. \tag{46}$$

Thus, the Eulerian characteristic frequency will be positive even when the covariance in the dissipation range is negative. The behavior of the Lagrangian characteristic frequency in the limit where $|\langle \phi'_\alpha\phi'_\beta\rangle_D^*|\to 0$ will depend on the behavior of the ratio $\langle \phi'_\alpha\phi'_\beta\rangle_{23}^*/\langle \phi'_\alpha\phi'_\beta\rangle_D^*$. We will explore this question further in Sec. V.

B. Scalar correlation coefficient

In the absence of mean scalar gradients (i.e., decaying scalar fields), the scalar correlation coefficient obeys[7]

$$\frac{1}{\rho_{\alpha\beta}}\frac{D\rho_{\alpha\beta}}{Dt}=-2\delta_{\alpha\beta}\langle r_{\alpha\beta}\rangle+\langle r_\alpha\rangle+\langle r_\beta\rangle, \tag{47}$$

where

$$\langle r_{\alpha\beta}\rangle=\frac{\langle \epsilon_{\alpha\beta}\rangle}{\langle \phi'_\alpha\phi'_\beta\rangle}. \tag{48}$$

As shown in Sec. V, the SR model predicts for large times a mechanical-to-scalar time-scale ratio of the form

$$R_\alpha=\frac{2\langle r_\alpha\rangle}{\langle\omega\rangle}\sim \mathrm{Sc}_\alpha^{-s}, \tag{49}$$

where s and the proportionality constant depend on the Reynolds number. Likewise, the SR model predicts the same form for the long-time behavior of the covariance mechanical-to-scalar time-scale ratio:

$$R_{\alpha\beta}=\frac{2\delta_{\alpha\beta}\langle r_{\alpha\beta}\rangle}{\langle\omega\rangle}=2C_D\,\mathrm{Re}_1\frac{\langle \phi'_\alpha\phi'_\beta\rangle_D}{\langle \phi'_\alpha\phi'_\beta\rangle}\sim \mathrm{Sc}_{\alpha\beta}^{-s}. \tag{50}$$

As discussed in Sec. V, finding a nonzero value for s is a direct result of the Sc-dependence of β_D. If $s=0$, then the time-scale ratios will be independent of the Schmidt numbers, and hence no long-term scalar decorrelation will be observed. The scalar correlation coefficient scales like

$$\frac{1}{\rho_{\alpha\beta}}\frac{D\rho_{\alpha\beta}}{Dt}\sim(\mathrm{Sc}_\alpha\,\mathrm{Sc}_\beta)^{-s/2}\left[\frac{1}{2}\left(\frac{\Gamma_\alpha}{\Gamma_\beta}\right)^{s/2}+\frac{1}{2}\left(\frac{\Gamma_\beta}{\Gamma_\alpha}\right)^{s/2}-\delta_{\alpha\beta}^s\right]. \tag{51}$$

We compare model results for this case with DNS data[7] in Sec. V. However, note that s is null in the absence of backscatter ($c_d=0$). Thus, backscatter combined with the Sc-dependence of β_D controls large-scale decorrelation in the SR model.

Besides backscatter and the Sc-dependent β_D, there is one other possible source of large-scale decorrelation: the molecular-diffusion constant C_d is smaller than its standard value (3) in Eq. (42) when $\mathrm{Sc}_\alpha\neq\mathrm{Sc}_\beta$. We rule out this possibility because it would cause the model to fail in the limit of pure diffusion where $\langle\varsigma\rangle_D=1$ and $\rho_{\alpha\beta}\to$constant>0. As discussed in the Appendix, this follows from the linearity of the scalar transport equation and is equivalent to assuming that the far-dissipation range of the scalar spectrum has a universal form when plotted using Batchelor scaling: $\kappa^*=\kappa/\kappa_D$.

C. Molecular mixing model

The LSR model described above provides a simple description of the distribution of covariance in spectral space. As shown in Sec. V, it is capable of describing much of the DNS data for differential diffusion in isotropic turbulence. Nevertheless, as it stands, it provides no information concerning the joint scalar pdf of ϕ_α^* and ϕ_β^*. For this purpose, a Lagrangian molecular mixing model must be formulated in terms of scalar statistics conditioned on the scalar values.

Constructing an appropriate model for molecular mixing is undoubtedly the most difficult task faced when applying pdf methods. For differential diffusion, the task is further complicated by the fact that correlation between the scalars must be successfully accounted for by the model. For example, the widely-employed IEM model[19] cannot be used because it fails to predict the correct evolution of the correlation coefficient. (Indeed, it predicts a constant value[7] for $\rho_{\alpha\beta}$ in the absence of mean scalar gradients!) In this work, we employ a Fokker–Planck model to describe two correlated Gaussian scalar fields. First, however, we will motivate the use of a Fokker–Plank type model by looking at some exact results for the stationary marginal and joint pdfs of two scalar fields.

The exact solution[33–37] for the marginal pdf of a homogeneous scalar field in the absence of a mean scalar gradient can be written in terms of the standardized scalar field,

$$V_\alpha=\frac{\phi'^*_\alpha}{\sigma_\alpha}, \tag{52}$$

where $\sigma_\alpha^2(t)=\langle\phi'^2_\alpha\rangle^*$, the standardized Lagrangian conditional scalar Laplacian,

$$\begin{aligned} g_\alpha(v_\alpha)&=\frac{\sigma_\alpha\langle\Gamma_\alpha\nabla^2\phi'_\alpha|V_\alpha=v_\alpha\rangle^*}{\langle\epsilon_\alpha\rangle^*}\\ &=\frac{\langle\Gamma_\alpha\nabla^2V_\alpha|V_\alpha=v_\alpha\rangle^*}{\langle r_\alpha\rangle^\dagger}, \end{aligned} \tag{53}$$

and the standardized Lagrangian conditional scalar dissipation rate,

$$n_\alpha(v_\alpha)=\frac{\langle \epsilon_\alpha|v_\alpha\rangle^*}{\langle \epsilon_\alpha\rangle^*}=\frac{1}{\langle r_\alpha\rangle^\dagger}\left\langle \Gamma_\alpha\frac{\partial V_\alpha}{\partial x_i}\frac{\partial V_\alpha}{\partial x_i}\middle| V_\alpha=v_\alpha\right\rangle^*. \quad (54)$$

(Note that the variables are standardized in terms of the Lagrangian conditional scalar variance and scalar dissipation rate provided by the LSR model.) Denoting the stationary marginal pdf by f_α^s, we have

$$f_\alpha^s(v_\alpha)=\frac{\mathcal{N}}{n_\alpha(v_\alpha)}\exp\left[\int\frac{g_\alpha(v_\alpha)}{n_\alpha(v_\alpha)}dv_\alpha\right], \quad (55)$$

where $\mathcal{N}$ is a normalization constant.

Although the stationary pdf given in Eq. (55) represents an exact solution, it does not provide a Lagrangian pdf model for the scalar. However, because it represents the stationary solution to a well-defined Fokker–Planck equation:[24]

$$\frac{\partial f_\alpha}{\partial t}=-\frac{\partial}{\partial v_\alpha}[\langle r_\alpha\rangle^\dagger g_\alpha(v_\alpha)f_\alpha]+\frac{\partial^2}{\partial v_\alpha^2}[\langle r_\alpha\rangle^\dagger n_\alpha(v_\alpha)f_\alpha], \quad (56)$$

a Lagrangian pdf model can be formulated in terms of a stochastic differential equation (SDE) with the same pdf:[24]

$$dV_\alpha=\langle r_\alpha\rangle^\dagger g_\alpha(V_\alpha)dt+\sqrt{2\langle r_\alpha\rangle^\dagger n_\alpha(V_\alpha)}dW(t), \quad (57)$$

where $dW(t)$ is a Wiener process. Then, by changing back to the nonstandardized scalar variables, a Lagrangian pdf model for ϕ'^*_α in the absence of mean scalar gradients results:

$$d\phi'^*_\alpha=\mathcal{V}_\alpha\phi'^*_\alpha dt+\langle\Gamma_\alpha\nabla^2\phi'_\alpha|\phi'^*_\alpha\rangle^*dt+\sqrt{2\langle\epsilon_\alpha|\phi'^*_\alpha\rangle^*}dW(t), \quad (58)$$

where

$$\mathcal{V}_\alpha=\frac{1}{2\langle\phi'^2_\alpha\rangle^*}\frac{D\langle\phi'^2_\alpha\rangle^*}{Dt}\bigg|_{S_\alpha=0} \quad (59)$$

is found from the LSR model in the absence of a scalar variance source term. For example, with $n_2=3$, this term becomes

$$\begin{aligned}\mathcal{V}_\alpha=&\alpha_1 f_1^c(\langle\mathfrak{s}_\alpha\rangle_1\Phi_\alpha^{-1}-\langle\mathfrak{s}_\alpha\rangle_1^*)+\alpha_{21}f_{21}^c(\langle\mathfrak{s}_\alpha\rangle_{21}\Phi_\alpha^{-1}\\&-\langle\mathfrak{s}_\alpha\rangle_{21}^*)+\alpha_{22}f_{22}^c(\langle\mathfrak{s}_\alpha\rangle_{22}\Phi_\alpha^{-1}-\langle\mathfrak{s}_\alpha\rangle_{22}^*)\\&+\alpha_{23}f_{23}^c(\langle\mathfrak{s}_\alpha\rangle_{23}\Phi_\alpha^{-1}-\langle\mathfrak{s}_\alpha\rangle_{23}^*)\\&+\gamma_D\langle r_\alpha\rangle_D(\Phi_\alpha^{-1}-1)-\langle r_\alpha\rangle^\dagger,\end{aligned} \quad (60)$$

where $f_{ij}^c=1-\kappa_{ij}/\kappa_U$. In the presence of a mean scalar gradient, an additional term appears on the right-hand side of Eq. (58) representing the conditional scalar flux $\langle u_i|\phi'^*_\alpha\rangle^*$. A closure for this term is presented below.

The idea presented above to model one scalar can be extended to model two scalars. The resultant Fokker–Planck equation for the joint pdf $f_{\alpha\beta}$ has drift coefficients defined in terms of the scalar Laplacians conditioned on both scalars:

$$A_\alpha(v_\alpha,v_\beta)=\frac{1}{\sigma_\alpha}\langle\Gamma_\alpha\nabla^2\phi'_\alpha|v_\alpha,v_\beta\rangle^*, \quad (61)$$

and a diffusion matrix defined in terms of the (joint) scalar dissipation rate conditioned on both scalars:

$$B_{\alpha\beta}(v_\alpha,v_\beta)=\frac{2}{\sigma_\alpha\sigma_\beta}\langle\epsilon_{\alpha\beta}|v_\alpha,v_\beta\rangle^*. \quad (62)$$

The SDE model requires us to write the diffusion matrix in the form[24]

$$\mathbf{B}=\mathbf{C}\mathbf{C}^T, \quad (63)$$

where T denotes the matrix transpose. This can be done by defining $\mathbf{C}$ as

$$\mathbf{C}=\begin{bmatrix}\sqrt{\langle\epsilon_\alpha|v_\alpha,v_\beta\rangle^*}\sigma_\alpha^{-1}C_1 & \sqrt{\langle\epsilon_\alpha|v_\alpha,v_\beta\rangle^*}\sigma_\alpha^{-1}C_2\\ \sqrt{\langle\epsilon_\beta|v_\alpha,v_\beta\rangle^*}\sigma_\beta^{-1}C_2 & \sqrt{\langle\epsilon_\beta|v_\alpha,v_\beta\rangle^*}\sigma_\beta^{-1}C_1\end{bmatrix}, \quad (64)$$

where

$$C_1(v_\alpha,v_\beta)=[1+(1-|g^\dagger_{\alpha\beta}|^2)^{1/2}]^{1/2}, \quad (65)$$

$$C_2(v_\alpha,v_\beta)=\frac{g^\dagger_{\alpha\beta}}{|g^\dagger_{\alpha\beta}|}[1-(1-|g^\dagger_{\alpha\beta}|^2)^{1/2}]^{1/2}, \quad (66)$$

and the Lagrangian conditional gradient correlation coefficient is defined by

$$g^\dagger_{\alpha\beta}(v_\alpha,v_\beta)=\frac{\langle\epsilon_{\alpha\beta}|v_\alpha,v_\beta\rangle^*}{\sqrt{\langle\epsilon_\alpha|v_\alpha,v_\beta\rangle^*\langle\epsilon_\beta|v_\alpha,v_\beta\rangle^*}}. \quad (67)$$

Note that if the scalar gradients are perfectly correlated with $g^\dagger_{\alpha\beta}=1$, then $C_1=C_2=1$ and the diffusion matrix has rank 1. This will result in perfectly correlated scalars. In the other extreme where $g^\dagger_{\alpha\beta}=0$, $C_1=\sqrt{2}$ and $C_2=0$ so that the diffusion matrix is diagonal. This will result in uncorrelated scalars.

The Lagrangian pdf model for two scalars then follows from the Fokker–Planck equation. Including the conditional scalar flux term, the SDEs become

$$\begin{aligned}d\phi'^*_\alpha=&-\langle u_i|\phi'^*_\alpha,\phi'^*_\beta\rangle^*\frac{\partial\langle\phi_\alpha\rangle}{\partial x_i}dt+\mathcal{V}_\alpha\phi'^*_\alpha dt\\&+\langle\Gamma_\alpha\nabla^2\phi'_\alpha|\phi'^*_\alpha,\phi'^*_\beta\rangle^*dt\\&+(\langle\epsilon_\alpha|\phi'^*_\alpha,\phi'^*_\beta\rangle^*)^{1/2}\left[C_1(\phi'^*_\alpha,\phi'^*_\beta)dW_\alpha(t)\right.\\&\left.+\left(\frac{\langle\phi'^2_\alpha\rangle^*}{\langle\phi'^2_\beta\rangle^*}\right)^{1/2}C_2(\phi'^*_\alpha,\phi'^*_\beta)dW_\beta(t)\right]\end{aligned} \quad (68)$$

and

$$\begin{aligned}d\phi'^*_\beta=&-\langle u_i|\phi'^*_\alpha,\phi'^*_\beta\rangle^*\frac{\partial\langle\phi_\beta\rangle}{\partial x_i}dt+\mathcal{V}_\beta\phi'^*_\beta dt\\&+\langle\Gamma_\beta\nabla^2\phi'_\beta|\phi'^*_\alpha,\phi'^*_\beta\rangle^*dt\\&+(\langle\epsilon_\beta|\phi'^*_\alpha,\phi'^*_\beta\rangle^*)^{1/2}\left[\left(\frac{\langle\phi'^2_\beta\rangle^*}{\langle\phi'^2_\alpha\rangle^*}\right)^{1/2}\right.\\&\times C_2(\phi'^*_\alpha,\phi'^*_\beta)dW_\alpha(t)\\&\left.+C_1(\phi'^*_\alpha,\phi'^*_\beta)dW_\beta(t)\right],\end{aligned} \quad (69)$$

where $dW_\alpha(t)$ and $dW_\beta(t)$ are uncorrelated Wiener processes. Note that this model can be extended to cases with more than two scalars. The remaining challenge is thus to find appropriate models for the conditional scalar Laplacians and the conditional (joint) scalar dissipation rates. Hereinafter we shall consider only Gaussian scalars.

D. Gaussian scalars

In Sec. V, we compare model predictions to DNS data for homogeneous scalar fields with and without uniform mean scalar gradients. Because such fields are nearly Gaussian, it suffices to consider the conditional statistics for only this case:

$$\langle \epsilon_\alpha | \phi'^*_\alpha, \phi'^*_\beta \rangle^* = \langle \epsilon_\alpha \rangle^*, \tag{70}$$

$$\langle \epsilon_{\alpha\beta} | \phi'^*_\alpha, \phi'^*_\beta \rangle^* = \langle \epsilon_{\alpha\beta} \rangle^*, \tag{71}$$

$$\langle \Gamma_\alpha \nabla^2 \phi'_\alpha | \phi'^*_\alpha, \phi'^*_\beta \rangle^* = a_{\alpha\alpha}\phi'^*_\alpha + a_{\alpha\beta}\phi'^*_\beta, \tag{72}$$

where

$$a_{\alpha\alpha} = -\langle r_\alpha \rangle^\dagger + \frac{\rho^\dagger_{\alpha\beta}[\langle r_{\alpha\beta}\rangle^\dagger(\sqrt{\mathrm{Sc}_\beta/\mathrm{Sc}_\alpha}+1) - 2\langle r_\alpha\rangle^\dagger]}{1-|\rho^\dagger_{\alpha\beta}|^2}\rho^\dagger_{\alpha\beta}, \tag{73}$$

$$a_{\alpha\beta} = \frac{\rho^\dagger_{\alpha\beta}[\langle r_{\alpha\beta}\rangle^\dagger(\sqrt{\mathrm{Sc}_\beta/\mathrm{Sc}_\alpha}+1) - 2\langle r_\alpha\rangle^\dagger]}{1-|\rho^\dagger_{\alpha\beta}|^2}\sqrt{\frac{\langle \phi'^2_\alpha\rangle^*}{\langle \phi'^2_\beta\rangle^*}}, \tag{74}$$

and

$$\rho^\dagger_{\alpha\beta} = \frac{\langle \phi'^2_{\alpha\beta}\rangle^*}{\sqrt{\langle \phi'^2_\alpha\rangle^*\langle \phi'^2_\beta\rangle^*}}. \tag{75}$$

Note that the LSR model provides all of the terms appearing in the Gaussian conditional statistics. Thus, the model equations will close at the Lagrangian pdf level once a model is chosen for the conditional scalar flux.

E. Scalar flux model

In a Lagrangian full pdf simulation of inhomogeneous turbulent scalar mixing,[38] the fluctuating velocity appears as a random variable, and thus no closure is required for the scalar flux. In isotropic turbulence, the mathematical description can be simplified — without affecting the predictions for differential diffusion — by employing a stochastic model for the scalar flux. For the Gaussian scalar fields considered in this work, we will use the following stochastic gradient-diffusion model that is valid for *uniform* mean scalar gradients:

$$-\langle u_i | \phi'^*_\alpha, \phi'^*_\beta \rangle^* \frac{\partial\langle\phi_\alpha\rangle}{\partial x_i} = \left(\frac{D_T}{2}\right)^{1/2}\left|\frac{\partial\langle\phi_\alpha\rangle}{\partial x_i}\right|[D_1 dW^s_\alpha(t) + D_2 dW^s_\beta(t)], \tag{76}$$

$$-\langle u_i | \phi'^*_\alpha, \phi'^*_\beta \rangle^* \frac{\partial\langle\phi_\beta\rangle}{\partial x_i} = \left(\frac{D_T}{2}\right)^{1/2}\left|\frac{\partial\langle\phi_\beta\rangle}{\partial x_i}\right|[D_2 dW^s_\alpha(t) + D_1 dW^s_\beta(t)], \tag{77}$$

where

$$D_1 = (1+|\sin(\theta_{\alpha\beta})|)^{1/2}, \tag{78}$$

$$D_2 = \frac{\cos(\theta_{\alpha\beta})}{|\cos(\theta_{\alpha\beta})|}(1-|\sin(\theta_{\alpha\beta})|)^{1/2}, \tag{79}$$

$\theta_{\alpha\beta}$ is the angle between the two mean scalar gradient vectors, and $dW^s_\alpha(t)$ and $dW^s_\beta(t)$ are uncorrelated Wiener processes.

Note that the Lagrangian time series for the scalars produced by the stochastic gradient-diffusion model will be highly fluctuating (due to the Wiener processes), and thus give a poor representation of Lagrangian time series for the scalars $\phi'^*(t)$ in turbulent flow. This would not be the case, however, if the full Lagrangian pdf model were employed wherein the Wiener processes are replaced by the fluctuating velocity field. Note, however, that the Lagrangian time series for the scalar dissipation rates presented in Sec. VI depend solely on $\omega^*(t)$ [Eq. (42)], and thus are independent of the choice of the model for the scalar flux.

V. COMPARISON WITH DNS DATA

A. Overview of numerical simulations

In stationary, homogeneous turbulence, the SR model reduces to a small set of ordinary differential equations (ODEs).[21] For convenience, the model can be rewritten in terms for the spectral fractions $\langle \varsigma_{\alpha\beta}\rangle_{ij}$ and the scalar frequencies $\langle r_{\alpha\beta}\rangle$. For two scalars, the total number of equations is then equal to $3\times$(number of spectral substages $+$scalar frequency). Thus, for $R_\lambda = 230$ $(n_2 = 4)$, a total of 21 ODEs are required. Assuming that the turbulence quantities are known, the SR model equations are easily solved using standard initial-value ODE routines. For inert scalars, the SR model suffices to describe differential-diffusion effects (i.e., in terms of the scalar variance and covariance spectrum).

The extension of the SR model to treat reacting scalars requires a Lagrangian pdf description formulated in terms of stochastic differential equations (SDEs). The number of coupled SDEs involved in the LSR model is the same as the number of ODEs in the SR model. In addition, a random model for the turbulent frequency $\omega^*(t)$ must be supplied (here it is described by a SDE[20]), and appears as the random driving force in the model equation for the scalar dissipation rate. [The LSR model reduces to the SR model by setting $\omega^*(t) = \langle\omega\rangle$.] Finally, for studies interested in the joint pdf of the two scalars, an appropriate mixing model (like the Fokker–Planck model employed in this study) can be solved using the scalar dissipation rates computed from the LSR model as inputs. In this work, the full set of coupled SDEs was simulated using the order 2.0 weak Taylor scheme described in Kloeden and Platen[39] with the time step chosen to be at least ten times smaller than the Kolmogorov time scale

TABLE II. Mechanical-to-scalar time-scale ratio as a function of Sc normalized by the value at Sc=1 for $R_\lambda=38$ and $c_b=1$.

Sc	0.25	0.50
DNS (Ref. 7)	1.10	1.06
LSRM	1.08	1.05

to ensure accurate solutions. Unless noted otherwise, all simulations employed 10^3 stochastic particles to estimate the ensemble averages. Thus, for $n_2=4$, each stochastic particle carried a vector of $21+1+2=24$ random variables whose values were determined by 24 SDEs. In general, it was found that the LSR model's predictions for the ensemble-averaged spectral quantities are in excellent agreement with the SR model's predictions for the same quantities.

B. Mechanical-to-scalar time-scale ratio

As seen from Eq. (47), the mechanical-to-scalar time-scale ratios R_α and $R_{\alpha\beta}$ are the key quantities for determining the decorrelation rate of two scalars in the absence of mean scalar gradients. In particular, if these ratios are independent of the Schmidt number [i.e., $s=0$ in Eq. (51)], then the scalar correlation will attain a constant, nonzero value after an initial transient phase, wherein only the dissipation-range scales decorrelate. DNS data[7] with forced isotropic turbulence indicate that R_α increases with decreasing Sc, and that the scalars decorrelate for large times. In the LSR model, the Sc dependence of the mechanical-to-scalar time-scale ratio is controlled by the function $h(\mathrm{Sc})$ in the backscatter rate β_D [Eq. (26)]. (This assumes that the backscatter parameter c_d is chosen to be nonzero.) Defining $h(\mathrm{Sc})$ as in Eq. (27) with $c_b=1$ yields satisfactory agreement with DNS data[7] for $R_\lambda=38$ and Sc=1/4 and 1/2, as shown in Table II. Results for four different Reynolds numbers ($R_\lambda=38$, 90, 160, and 230) are presented in Fig. 1. Note that the time-scale ratios for fixed R_λ fall nearly on a line when plotted against Sc. Note also that for a fixed number of inertial-range substages n_2, the time-scale ratio is nearly independent of the Reynolds number. This is a result of ''lumping'' all wavenumbers in a substage into discrete, instead of continuous, variables. Figure 1 can be used to determine both R_α and $R_{\alpha\beta}$ by setting $\mathrm{Sc}=\mathrm{Sc}_\alpha$ and $\mathrm{Sc}=\mathrm{Sc}_{\alpha\beta}$, respectively. A perfectly linear relationship between $\ln(R)$ and $\ln(\mathrm{Sc})$ would result in Eq. (51) where $-s$ is the slope on a log–log plot. The steady-state mechanical-to-scalar time-scale ratio in the presence of a uniform mean scalar gradient as a function of Sc is shown in Fig. 2 (again with $c_b=1$). Note that the behavior is very similar to that seen for decaying scalars. The only obvious difference is increased curvature.

In the LSR model, backscatter is required to correctly predict the observed dependence of the mechanical-to-scalar time-scale ratio on the Reynolds number. The key parameter controlling backscatter is c_d. In theory, c_d can be determined by studying spectral transport for a single scalar with Sc=1. Alternatively, the time dependence of the coherency spectrum[7,11,15] for two scalars with $\mathrm{Sc}_\alpha=\mathrm{Sc}_\beta=1$ that are initially perfectly correlated for all but a subrange of wavenumbers can be employed to fix c_d. DNS data[7] for this case are available for $R_\lambda=38$, where it can be seen (Fig. 11 in Yeung and Pope[7]) that the ''banded'' coherency spectrum[7] relaxes to its final self-similar form in approximately three eddy-turnover times (T_E). (See the Appendix for an exact definition of the coherency spectrum.) Using the variables in the LSR model, the ''banded'' coherency spectrum can be defined as

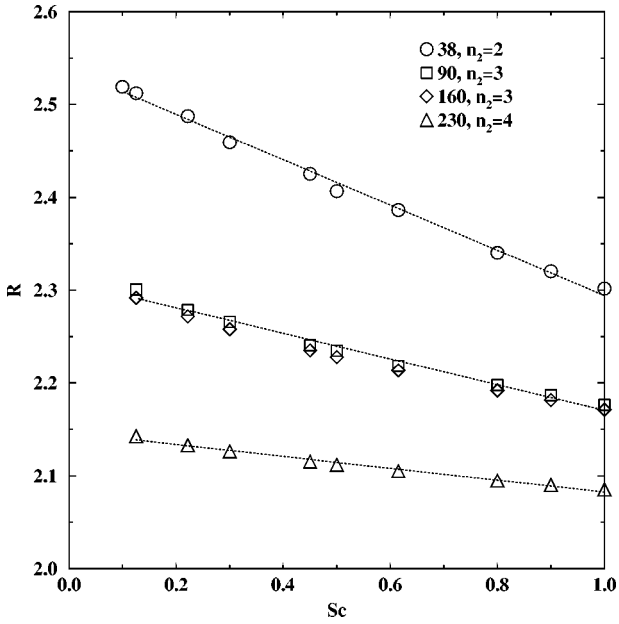

FIG. 1. Mechanical-to-scalar time-scale ratio for a decaying passive scalar as a function of Sc for four different Reynolds numbers ($R_\lambda=38$ ○, 90 □, 160 ◇, and 230 △) with $c_b=1$. Linear regression curves are given by the dotted lines with slopes that depend on the number of inertial-range substages.

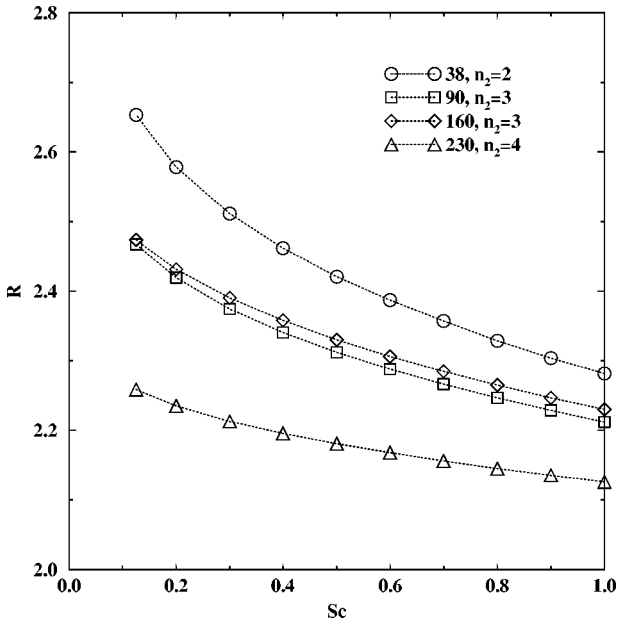

FIG. 2. Mechanical-to-scalar time-scale ratio for a passive scalar with a uniform mean gradient as a function of Sc for four different Reynolds numbers (R_λ = 38 ○, 90 □, 160 ◇, and 230 △) with $c_b=1$.

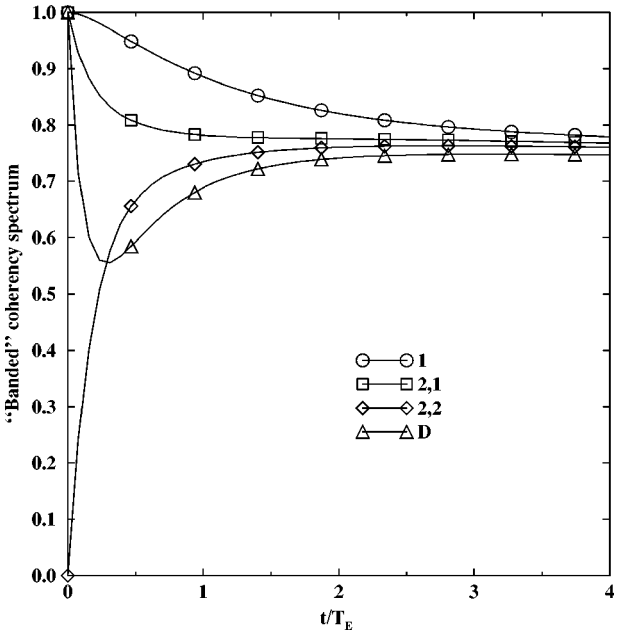

FIG. 3. ''Banded'' coherency spectrum for two scalars with $\mathrm{Sc}_\alpha=\mathrm{Sc}_\beta=1$. The fields are initially uncorrelated only in inertial subrange (2,2). Note that decorrelation is first transferred forward to small scales (D) before being backscattered to large scales (1).

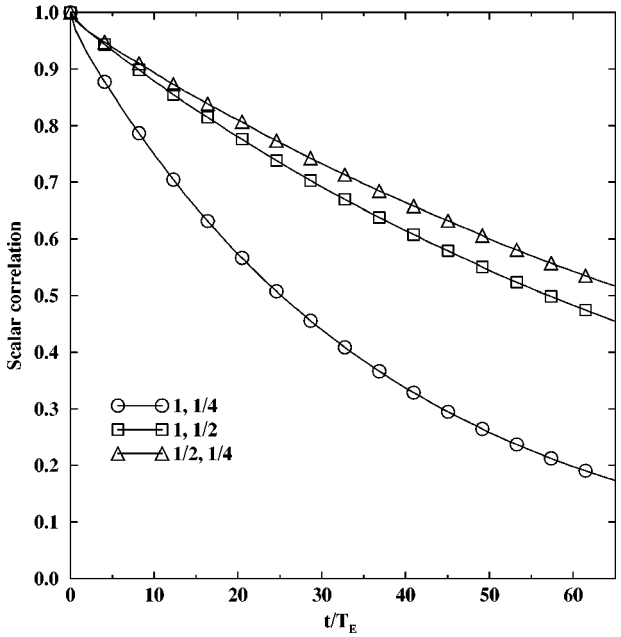

FIG. 4. Evolution of scalar correlation $\rho_{\alpha\beta}$ for decaying scalar fields at $R_\lambda=38$. Sc=(1,1/4) ○, (1,1/2) □, and (1/2,1/4) △.

$$b_{ij}(t)=\frac{\langle\phi'_\alpha\phi'_\beta\rangle_{ij}}{\sqrt{\langle\phi'^2_\alpha\rangle_{ij}\langle\phi'^2_\beta\rangle_{ij}}}. \tag{80}$$

(No summation over i or j is implied. Strictly speaking, this definition is invalid for $j=n_2$ and for the dissipation range where the cut-off wavenumbers depend on Sc.) Setting $b_{ij}(0)$ equal to unity for all wavenumber bands except $b_{22}(0)=0$, the parameter c_d then controls the time evolution of $b_{ij}(t)$. For example, with $c_d=0$ the cascade of coherency from large scales occurs unimpeded by backscatter, and $b_{22}\to 1$. On the other hand, if c_d is too large, then backscatter will quickly decorrelate large scales so that the final value of the correlation coefficient will be too small. The time evolution of the ''banded'' coherency spectrum for $R_\lambda=38$ with $c_d=1$ is shown in Fig. 3. As seen from DNS,[7] the small scales (b_D) decorrelate first due to forward transport. In contrast, the large scales decorrelate more slowly and reach their final values in approximately three to four eddy-turnover times. All results presented hereinafter were found with $c_d=1$.

C. Differential-diffusion effects for decaying scalars

Yeung and coworkers[7–9] have extensively studied differential-diffusion effects for decaying, Gaussian scalars in forced, isotropic turbulence using DNS. LSR model results can be directly compared with the DNS data by fixing R_λ and the Schmidt number pair $\mathrm{Sc}=(\mathrm{Sc}_\alpha,\mathrm{Sc}_\beta)$, and by knowing the relationship between T_E and $t_1=1/\langle\omega\rangle$. ($T_E$ is used to make t dimensionless.) The values of $T_E\langle\omega\rangle$ for the Reynolds numbers used in the DNS studies are given in Table III. For $R_\lambda=38$, the DNS study[7] employed three scalars with Sc=1, 1/2, and 1/4. Model results for the scalar correlation $\rho_{\alpha\beta}$ and the scalar-gradient correlation $g_{\alpha\beta}$ are shown in Figs. 4 and 5, respectively. The agreement with the DNS data[7] is satisfactory, including the dependence on the Schmidt number for fixed $\delta_{\alpha\beta}$ [i.e., Sc=(1,1/2) versus (1/2,

TABLE III. The relationship between the eddy-turnover time T_E and the turbulence frequency $\langle\omega\rangle$ as a function of R_λ for DNS studies.[26]

R_λ	38	90	160	230
$T_E\langle\omega\rangle$	0.513	0.331	0.278	0.270

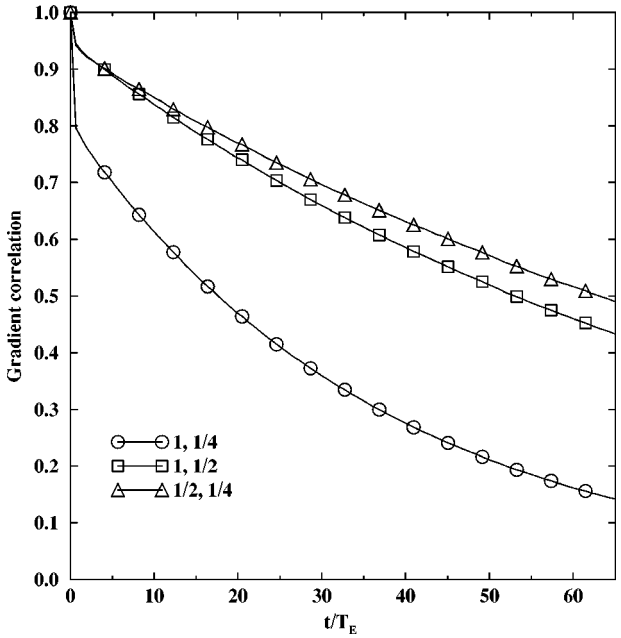

FIG. 5. Evolution of scalar-gradient correlation $g_{\alpha\beta}$ for decaying scalar fields at $R_\lambda=38$. Sc=(1,1/4) ○, (1,1/2) □, and (1/2,1/4) △.

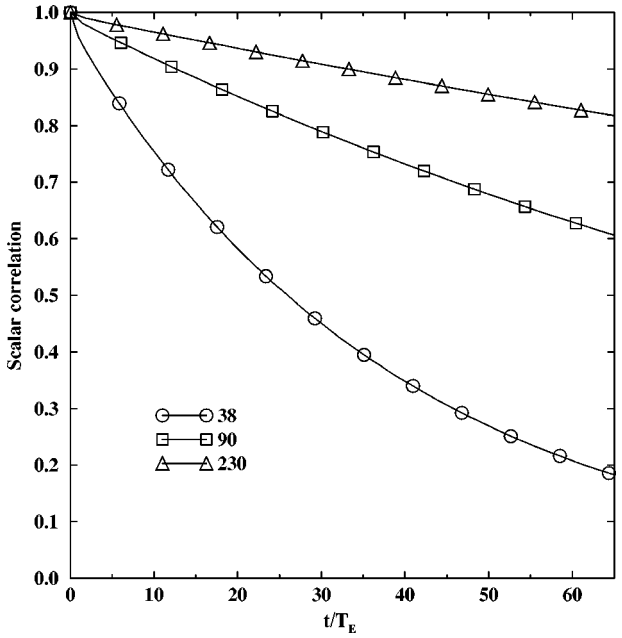

FIG. 6. Evolution of scalar correlation $\rho_{\alpha\beta}$ for decaying scalar fields as a function of R_λ with Sc=(1,1/4). As in Fig. 1, the number of inertial-range substages is the key parameter in determining the correlation decay rate.

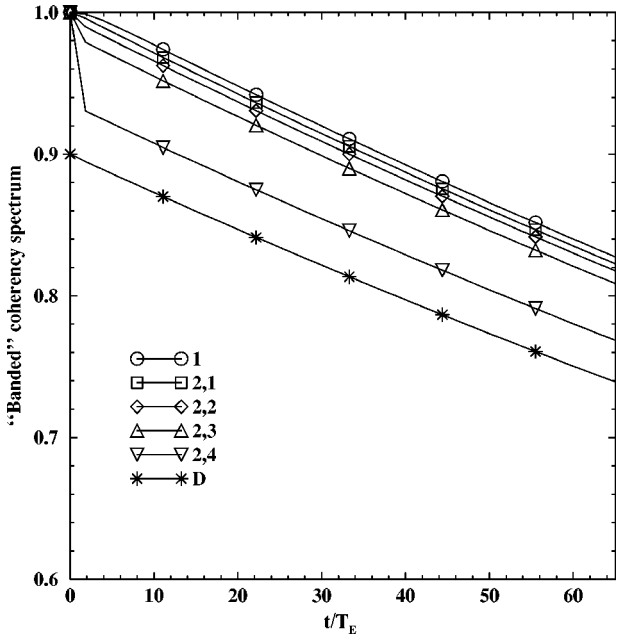

FIG. 7. Evolution of the ''banded'' coherency spectrum for decaying scalar fields at $R_\lambda=230$ with Sc=(1,1/4). Note that the spectrum quickly attains a self-similar form before undergoing a slow decay towards complete decorrelation.

1/4)]. At higher Reynolds numbers (e.g., $R_\lambda=230$), the correlation depends only on $\delta_{\alpha\beta}$. The parameter c_b also influences the correlation decay rate. The choice $c_b=1$ yields satisfactory agreement with DNS data for differential diffusion as well as for the mechanical-to-scalar time-scale ratio (Table II).

The dependence of the scalar correlation on the Reynolds number is illustrated in Fig. 6 for Sc=(1,1/4). The observed decrease in the decorrelation rate can be attributed to two factors: (1) $T_E\langle\omega\rangle$ decreases towards an asymptotic value with increasing R_λ; and (2) the exponent s in Eq. (51) decreases with increasing R_λ. For a large-enough Reynolds number, only (2) will be important. From the simulation data, the decay rate of the scalar correlation is found to scale with Reynolds number like

$$\frac{1}{\rho_{\alpha\beta}}\frac{D\rho_{\alpha\beta}}{Dt}\sim R_\lambda^{-0.6}\sim \mathrm{Re}^{-0.3}, \tag{81}$$

where Re is the integral-scale Reynolds number. The Reynolds-number exponent (0.3) predicted by the LSR model is less than the value (0.5) that might be expected based on classical spectral arguments.[17] The difference, however, can be attributed to backscatter: if $c_d=0$ (no backscatter) all decorrelation would be confined to the dissipation range which scales like $\mathrm{Re}^{-1/2}$. With backscatter, decorrelation ''leaks'' back to larger scales which decrease more slowly with an increasing Reynolds number, thereby decreasing the exponent. We will return to this question below when we look at the difference spectrum.

In Fig. 7, the time evolution of the ''banded'' coherency spectrum is shown for $R_\lambda=230$ and Sc=(1,1/4). As seen in DNS,[7,11,15] the coherency spectrum quickly attains a self-similar form, where the small scales are decorrelated more than the large scales, followed by a slow decorrelation of all scales towards complete decorrelation. In the self-similar state, the relative decorrelation of different wavenumber bands depends only on $\delta_{\alpha\beta}$ (i.e., is independent of the Reynolds number). Similar behavior is seen in DNS data[11,15] for the coherency spectrum. Finally, in Fig. 8 we illustrate the relative importance of backscatter (c_d) versus turbulent fluctuations [$\sigma(t)$] in determining the scalar decorrelation. The scatterplots in the first column were found with $c_d=1$, while those in the second column were found with $c_d=0$. Like-

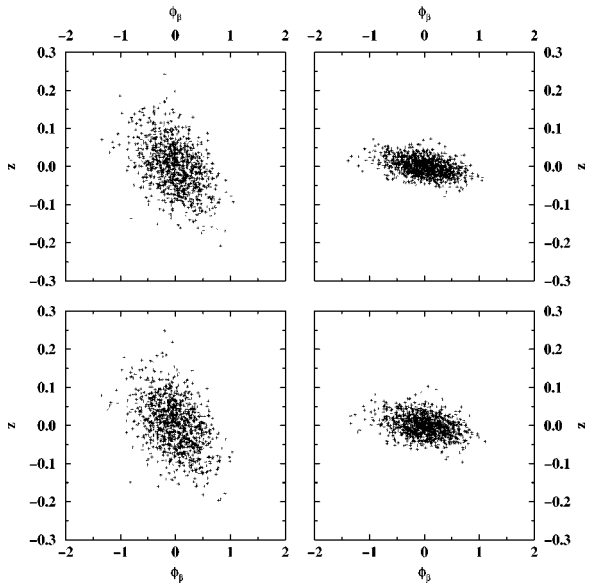

FIG. 8. Scatterplots of the scalar difference z versus ϕ_β at a fixed time t for Sc=(1,1/8). The decaying scalar fields were initially perfectly correlated. Top row: SR model ($\sigma(t)=1$). Bottom row: LSR model. First column: $c_d=1$. Second column: $c_d=0$.

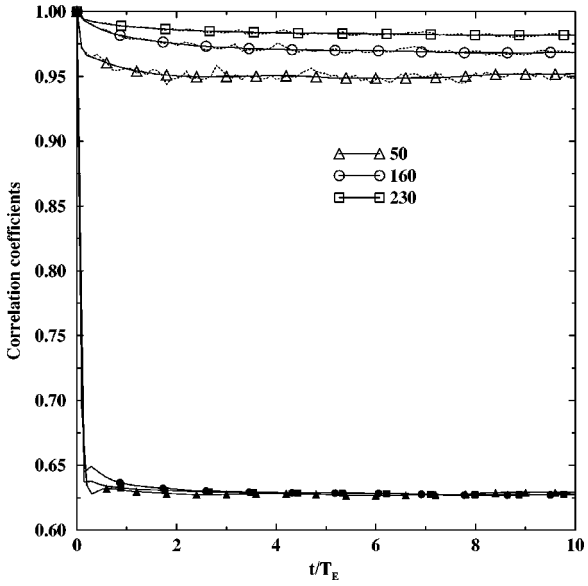

FIG. 9. Evolution of the correlation coefficients as a function of Reynolds number for Sc=(1,1/8). The uniform mean scalar gradients are colinear and $S_\alpha = S_\beta = 1$. Open symbols: scalar correlation. Closed symbols: gradient correlation. $R_\lambda = 230$ □, 160 ○, and 50 △. Solid lines: LSR model. Dashed lines: ensemble average of 1000 notional particles.

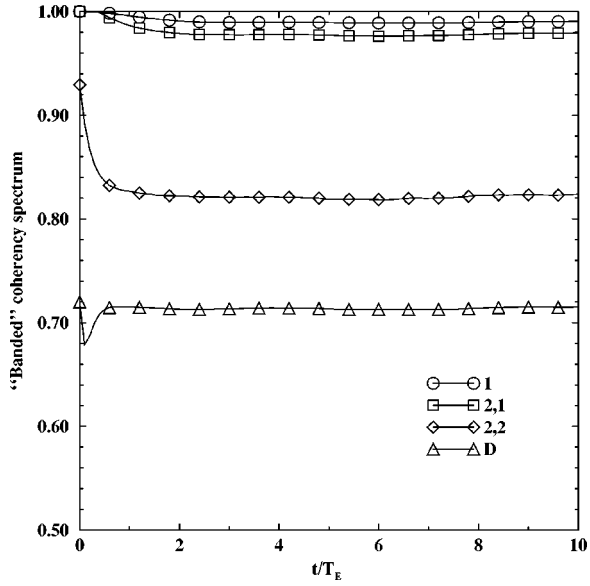

FIG. 10. Evolution of the ''banded'' coherency spectrum for Sc=(1,1/8), and $R_\lambda = 50$. The uniform mean scalar gradients are colinear and $S_\alpha = S_\beta = 1$.

wise, the scatterplots in the first row were found without turbulent fluctuations $[\sigma(t)=1]$, while those in the second row were found with turbulent fluctuations. All scatterplots correspond to the exact same time starting from identical initial conditions. Following Nilsen and Kosály,[13] we plot the difference $z=\phi_\alpha-\phi_\beta$ versus ϕ_β, where the latter is the more diffusive scalar. It is clear from the scatterplots that backscatter is the more important factor in predicting the correct decorrelation rate. Indeed, as noted earlier, with $c_d = 0$ decorrelation is confined to small scales, and thus $\rho_{\alpha\beta}$ does not decay to zero for large times. (In Fig. 8, the plots in the second column have reached their maximum decorrelation, while those in the first column will continue to decorrelate.) This is exactly the behavior seen with pure diffusion and is in qualitative agreement with Fig. 19 in Nilsen and Kosály.[13]

D. Differential-diffusion effects with a uniform mean scalar gradient

Another case of practical and theoretical interest is differential diffusion in the presence of uniform mean scalar gradients. In many ways, this case is easier to study than decaying scalars using DNS because the scalar fields quickly attain a statistically-stationary state in forced, isotropic turbulence.[9,11,15] The same is true for the LSR model. Typical results for the correlation coefficients are shown in Fig. 9 for Sc=(1,1/8) at three different Reynolds numbers. (Unless stated otherwise, we assume that the mean scalar gradients are colinear with unit magnitude and $D_T=1$. These assumptions only affect the magnitude of, for example, the scalar (co)variances, but not dimensionless quantities such as the correlation coefficients.) As noted in the Introduction [Eq. (13)], the gradient correlation approaches a constant value $g_{\alpha\beta}=1/\delta_{\alpha\beta}=0.629$, independent of the Reynolds number. On the other hand, the scalar correlation $\rho_{\alpha\beta}$ decreases with increasing Reynolds number. (We will look more closely at the Reynolds-number scaling further below.) Yeung[15] has presented similar data from DNS for Sc=(1,1/8) with the same Reynolds numbers. The agreement is, in general, satisfactory, with the DNS data showing perhaps slightly more decorrelation at the same R_λ. For a comparison, both the correlation coefficient found by summing the variables $\langle \phi'_\alpha \phi'_\beta \rangle_{ij}$ in the LSR model (solid lines), and by taking an ensemble average over 100 notational particles governed by the Fokker–Planck molecular mixing model [Eqs. (68) and (69)] (dashed lines) are shown in Fig. 9. (No variance reduction techniques have been used to force the second-order statistics to exactly agree with the LSR model.)

Other examples of LSR model results are shown in Figs. 10 and 11. In the former, the ''banded'' coherency spectrum is shown for $R_\lambda=50$ and Sc=(1,1/8). As seen in DNS,[11] the ''banded'' coherency spectrum quickly attains a stationary state wherein the large scales are nearly perfectly correlated, while the small scales are strongly decorrelated. In the LSR model, correlation is generated by the mean-gradient source terms $\gamma_{2j}S_{\alpha\beta}$. Because $\gamma_{21}\sim 1$ while $\gamma_{2\,n_2}\sim 1/R_\lambda$, most of the correlation flows into large scales and, hence, they remain more correlated. In Fig. 11, the scalar correlations for three Schmidt-number pairs at $R_\lambda=90$ are shown. The Schmidt numbers were chosen to be similar to those used in a DNS study[9] with the same Reynolds number. Again, the agreement with the DNS data is satisfactory, with the model predicting a slightly higher correlation for the same Schmidt-number pair. This can be partially attributed to the dependence of the scalar correlation on n_2, instead of R_λ (i.e., Fig. 2). For $n_2=3$, the comparison with DNS data[15] is much more favorable at $R_\lambda=160$.

In addition to the correlation coefficients, another variable of interest in differential-diffusion studies[5,12,13,6] is the

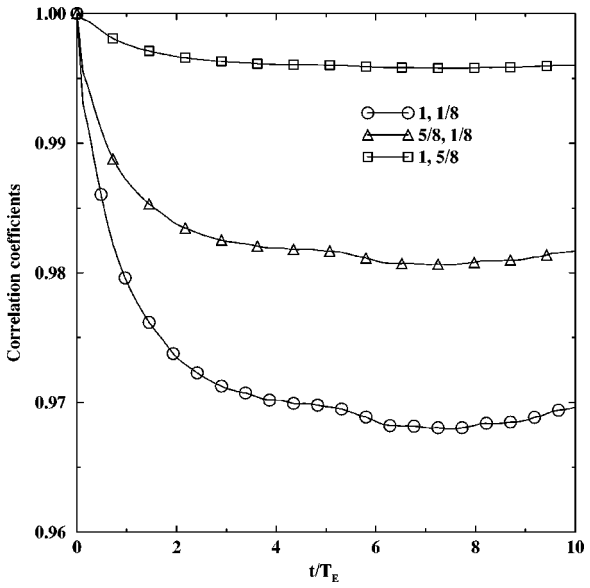

FIG. 11. Evolution of the scalar correlation for $R_\lambda = 90$. The uniform mean scalar gradients are colinear and $S_\alpha = S_\beta = 1$. Sc=(1,5/8) □, (5/8,1/8) △, and (1,1/8) ○.

scalar difference z. In particular, it is of interest to know how the difference variance,

$$\langle z^2 \rangle = \langle \phi_\alpha'^2 \rangle + \langle \phi_\beta'^2 \rangle - 2\langle \phi_\alpha' \phi_\beta' \rangle, \tag{82}$$

scales as a function of the Reynolds and Schmidt numbers. Data for the stationary second-order statistics predicted by the LSR model for Sc=(1,1/8) at three different Reynolds numbers (chosen so that n_2 varies from two to four) are given in Table IV. On a log–log plot, the difference variance versus R_λ falls nearly on a line so that $\langle z^2 \rangle \sim R_\lambda^{-0.6}$. Similar data for $R_\lambda = 230$ and various values of $\delta_{\alpha\beta}$ are given in Table V. (At high Reynolds numbers, the model results depend on the Schmidt numbers only through $\delta_{\alpha\beta}$.) From these data, the LSR model predicts the following scaling law for the difference variance:

$$\langle z^2 \rangle \sim g(\delta_{\alpha\beta}) R_\lambda^{-0.6} \sim g(\delta_{\alpha\beta}) \mathrm{Re}^{-0.3}, \tag{83}$$

where $g(x) = 0.0869(x-1) - 0.0553(x-1)^2$ for $1 \leqslant x \leqslant 1.6$ (see Table V).

The fact that the exponent of the Reynolds-number dependence of the difference variance is less than 0.5 is linked to backscatter in the LSR model. One way to look at backscatter is through the normalized ''banded'' difference spectrum,[7] defined in terms of the LSR model variables by

$$F_{ij}(t) = \frac{\langle \phi_\alpha'^2 \rangle_{ij} + \langle \phi_\beta'^2 \rangle_{ij} - 2\langle \phi_\alpha' \phi_\beta' \rangle_{ij}}{\langle z^2 \rangle}. \tag{84}$$

At very short times, all decorrelation is confined to small scales so that $F_D(0) = 1$. DNS data[7] show that at later times the difference spectrum reaches a nearly self-similar form with considerable energy at intermediate scales. LSR model results for $R_\lambda = 230$ and Sc=(1,1/8) are shown in Fig. 12. From this figure, it can be seen that while most of the energy remains at small scales, considerable transfer to large scales occurs. For comparison, the steady-state covariance energy fractions $\langle \varsigma_{\alpha\beta} \rangle_{ij}$ are given in Table VI, along with the ratio $F_{ij}/\langle \varsigma_{\alpha\beta} \rangle_{ij}$. From the ratios, it can be seen that inertial substage (2,3) contains a nearly two-fold excess of difference energy as compared to the covariance spectrum. Likewise, the difference energy in inertial substage (2,2) is the same as for the covariance spectrum. In the LSR model, these ratios (and hence the exponent of the Reynolds-number depen-

TABLE IV. Stationary second-order scalar statistics as a function of Reynolds number for Sc=(1,1/8). The turbulence is taken to be stationary with $\langle \omega \rangle = 1$ and $D_T = 1$. The scalar fields have colinear uniform mean gradients of unit magnitude so that $S_\alpha = S_\beta = S_{\alpha\beta} = 1$. The difference scalar field is defined by $z = \phi_\alpha - \phi_\beta$. Note that $\langle z^2 \rangle \sim R_\lambda^{-0.6}$.

R_λ	50	90	230
$\langle \phi_\alpha'^2 \rangle$	0.900	0.933	0.965
$\langle \phi_\beta'^2 \rangle$	0.766	0.833	0.899
$\langle \phi_\alpha' \phi_\beta' \rangle$	0.790	0.855	0.916
$\langle z^2 \rangle$	0.087	0.057	0.034

TABLE V. Stationary second-order scalar statistics as a function of $\delta_{\alpha\beta}$ for $\mathrm{Sc}_\alpha = 1$ and $R_\lambda = 230$. The other parameters are the same as in Table IV. In this range of Schmidt numbers, $\langle z^2 \rangle = 0.0869(\delta_{\alpha\beta}-1) - 0.0553(\delta_{\alpha\beta}-1)^2$.

Sc_β	1/2	1/3	1/4	1/5	1/6	1/7	1/8
$\delta_{\alpha\beta}$	1.061	1.155	1.25	1.342	1.429	1.512	1.591
$\langle \phi_\alpha'^2 \rangle$	0.959	0.967	0.966	0.966	0.966	0.965	0.965
$\langle \phi_\beta'^2 \rangle$	0.937	0.924	0.916	0.910	0.906	0.902	0.899
$\langle \phi_\alpha' \phi_\beta' \rangle$	0.944	0.939	0.931	0.926	0.922	0.918	0.816
$\langle z^2 \rangle$	0.007	0.014	0.019	0.024	0.028	0.031	0.034

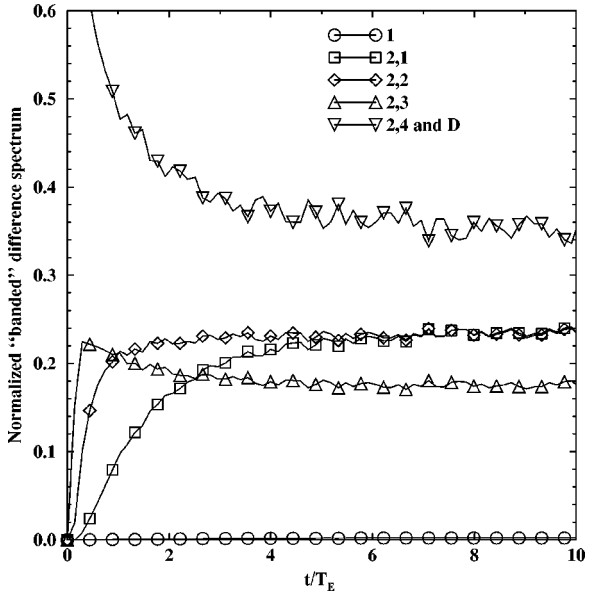

FIG. 12. Evolution of the normalized ''banded'' difference spectrum for Sc=(1,1/8) and $R_\lambda = 230$. Collinear uniform mean scalar gradients are applied with $S_\alpha = S_\beta = 1$. The data are normalized by dividing them by $\langle z^2 \rangle(t)$, and thus represent the fraction of the difference spectrum in each wavenumber band. These values are compared to the steady-state spectral fractions for the cospectrum in Table VI.

TABLE VI. Steady-state scalar energy fractions for $R_\lambda = 230$ and Sc $= (1,1/8)$.

(i,j)	1	(2,1)	(2,2)	(2,3)	(2,4) and D
F_{ij}	0.001	0.24	0.24	0.18	0.34
$\langle s_{\alpha\beta}\rangle_{ij}$	0.01	0.56	0.23	0.10	0.10
Ratio	0.1	0.4	1.0	1.8	3.4

dence) are controlled by the amount of backscatter. From the DNS data for the difference spectrum,[7,15] it is clear that backscatter plays a critical role in determining the shape of the spectrum, and that it must be included in any successful multi-scale model for differential diffusion.

Finally, as an example of the LSR model's ability to successfully handle a sudden change in the orientation of the mean scalar gradients, results for such a case are presented in Fig. 13. For this calculation, we have again let $R_\lambda = 230$ and Sc$=(1,1/8)$. Initially the scalar fields are uncorrelated and colinear mean scalar gradients with the same orientation are applied. The scalar fields respond by moving towards a positive correlation for both the scalars and their gradients. (The dashed lines represent ensemble averages over 100 notional particles.) At $t = 7.4T_E$ the orientation of the gradients is reversed. The scalar fields immediately respond by moving towards negative correlation. From the figure, it can be seen that the small scales respond more rapidly than the large scales so that at one point the gradient correlation is negative when the scalar correlation is still positive. As noted in Sec. IV, the LSR model successfully handles this potential singularity in the scalar time scale by employing $\langle r_{\alpha,\beta}\rangle_D^\dagger$ [Eq. (43)] instead of $\langle r_{\alpha,\beta}\rangle^\dagger$ [Eq. (44)]. The former always remains positive and well behaved, even at points where the scalar covariance is null.

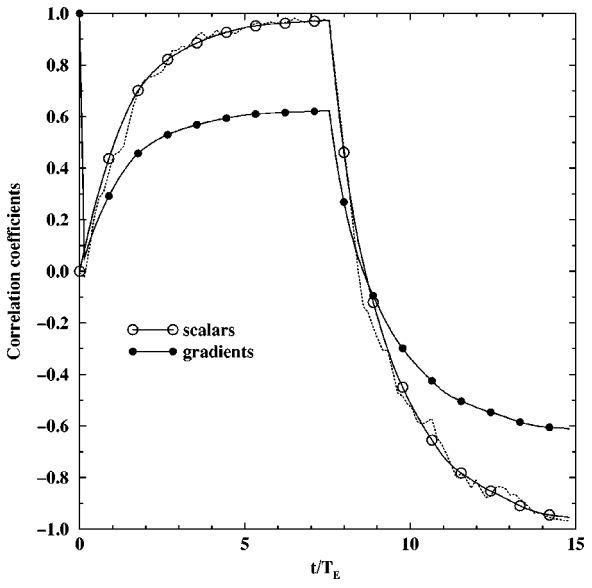

FIG. 13. Evolution of the correlation coefficients for initially uncorrelated scalar fields with Sc$=(1,1/8)$, and $R_\lambda = 230$. The uniform mean scalar gradients are initially colinear with $S_{\alpha\beta} = 1$. At $t\langle\omega\rangle = 2$, the mean scalar gradients are reversed so that $S_{\alpha\beta} = -1$. Note that although the correlation functions do not pass through zero correlation at the same time, the model remains numerically stable. The dashed line corresponds to the ensemble average of 100 notional particles.

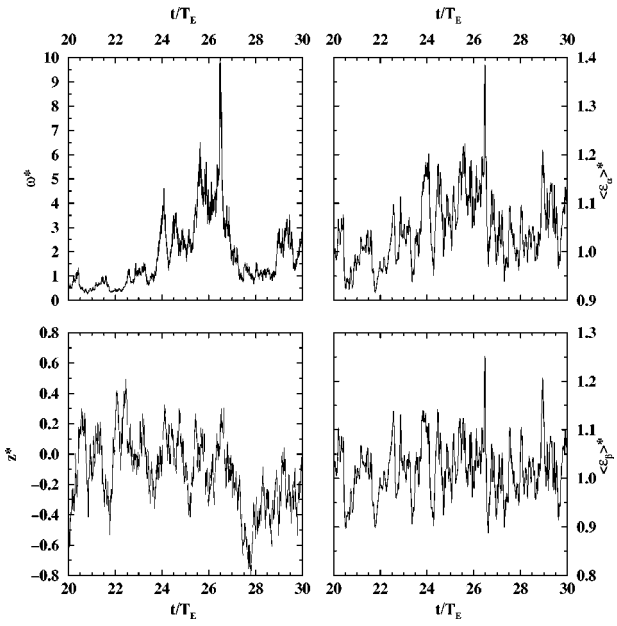

FIG. 14. Stationary Lagrangian time series following a notional particle at $R_\lambda = 230$. Top left: normalized turbulence dissipation rate $\omega^*(t)/\langle\omega\rangle$. Bottom left: scalar difference $z^*(t)$. Top right: normalized scalar dissipation rate $\langle\epsilon_\alpha\rangle^*(t)/\langle\epsilon_\alpha\rangle$ for scalar with Sc$=1$. Bottom right: normalized scalar dissipation rate $\langle\epsilon_\beta\rangle^*(t)/\langle\epsilon_\beta\rangle$ for scalar with Sc$=1/8$. Time series were allowed to become statistically stationary before collecting data.

E. Lagrangian time series

The results discussed to this point are all Eulerian statistics and could be found without resorting to a Lagrangian pdf description (i.e., by using the SR model). The LSR model provides considerably more information that will be important, for example, in applications where fluctuations in the scalar dissipation rate lead to local extinction of chemical reactions.[40–44] In Fig. 14 typical Lagrangian time series following a single notional particle[38] are shown for $R_\lambda = 230$ and Sc$=(1,1/8)$. In the top-left figure, the turbulence frequency $\omega^*(t)$ is plotted. The large fluctuations away from the mean value (1) are typical of stochastic processes whose marginal pdfs have exponential tails.[20] The turbulence frequency is the driving force for fluctuations in the Lagrangian conditional scalar dissipation rates shown in the right-hand column of Fig. 14. Note, however, that the magnitude of the fluctuations in the scalar dissipation rate is considerably smaller than those of the turbulence frequency. This is due to the ''low-pass'' filtering effect of the molecular dissipation term in the model equations [e.g., Eq. (38)]. Moreover, it can be noted that the fluctuations in $\langle\epsilon_\beta\rangle^*$ (i.e., the more diffusive scalar) are smaller than for $\langle\epsilon_\alpha\rangle^*$. Presumably, this can be attributed to stronger damping by the molecular diffusion term for the more diffusive scalar. The time series for the scalar difference shown on the bottom-left of Fig. 14 is typical of a Gaussian random process generated by a linear

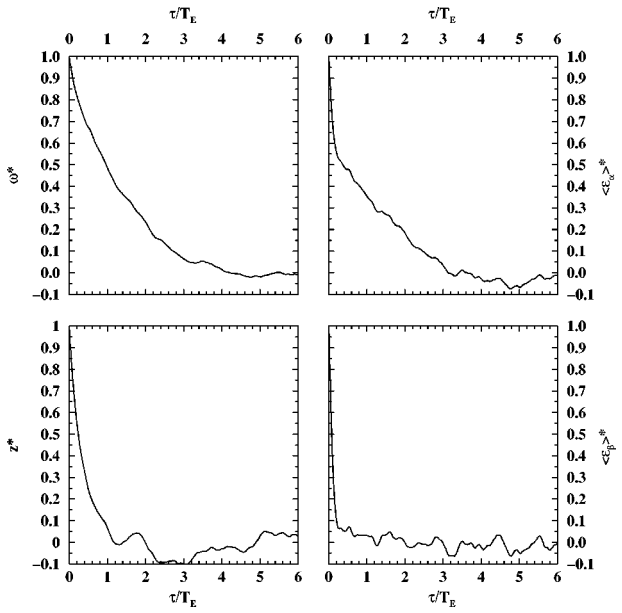

FIG. 15. Auto-correlation functions found from Lagrangian time series like those in Fig. 14. Estimates were computed based on data collected over a time interval of length $148T_E$.

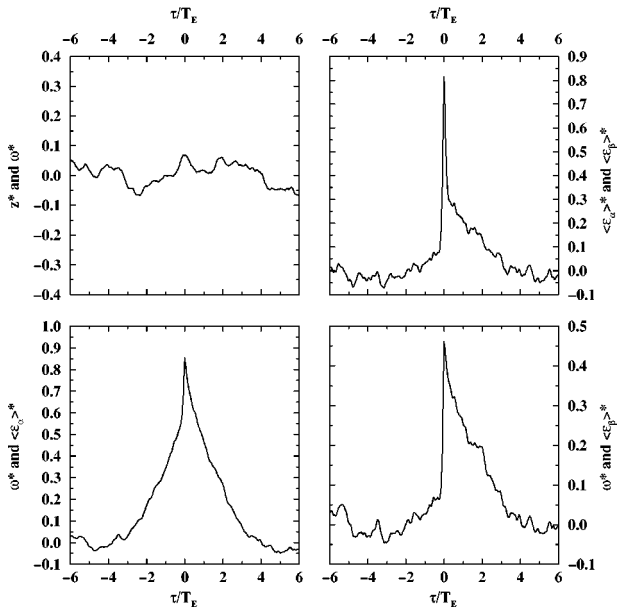

FIG. 16. Cross-correlation functions for selected Lagrangian time series in Fig. 14. Top left: $z^*(t)$ and $\omega^*(t+\tau)$. Top right: $\langle\epsilon_\alpha\rangle^*(t)$ and $\langle\epsilon_\beta\rangle^*(t+\tau)$. Bottom left: $\omega^*(t)$ and $\langle\epsilon_\alpha\rangle^*(t+\tau)$. Bottom right: $\omega^*(t)$ and $\langle\epsilon_\beta\rangle^*(t+\tau)$.

SDE.[24] Moreover, because the scalar fields are Gaussian, we can expect (shown below) that z^* will be independent of the other random variables shown in Fig. 14.

In assessing the importance of scalar dissipation rate fluctuations on chemical reactions, an important quantity will be their ''characteristic lifetime'' relative to the reaction time scales. One measure of the lifetime of Lagrangian fluctuations is the Lagrangian correlation time found by integrating over the Lagrangian auto-correlation function.[24] The latter is defined for a stationary Lagrangian time series $T^*(t)$ with $\langle T\rangle=0$ by

$$\rho_{TT}(\tau)=\frac{\langle T^*(t)T^*(t+\tau)\rangle}{\langle T^2\rangle}. \tag{85}$$

In Fig. 15, auto-correlation functions found for the Lagrangian time series in Fig. 14 are presented. As expected,[20] the auto-correlation function for the turbulence frequency falls off nearly exponentially with a correlation time of approximately $1.4T_E$. Likewise, the auto-correlation functions for the scalars (not shown) and for the scalar difference (bottom left) fall off nearly exponentially. However, the correlation times of the scalars (both approximately $1.6T_E$) are much larger than the correlation time for the scalar difference (approximately $0.35T_E$). Presumably, this reflects the fact that the difference spectrum (Fig. 12) contains more energy at small (fast) scales than the scalar spectra. The behavior of the auto-correlation functions for the Lagrangian scalar dissipation rates shown in the right-hand column of Fig. 15 is slightly more complicated. For the less-diffusive scalar (ϕ_α), the dissipation auto-correlation function falls quickly to 0.5 before dropping off quasi-exponentially towards zero. Its correlation time is approximately $0.7T_E$. For the more-diffusive scalar, the dissipation auto-correlation function drops almost immediately to zero yielding a correlation time of approximately $0.1T_E$.

The interactions between the various model variables can be studied by computing the cross-correlation function between two stationary Lagrangian time series:

$$\rho_{T_1T_2}(\tau)=\frac{\langle T_1^*(t)T_2^*(t+\tau)\rangle}{\sqrt{\langle T_1^2\rangle\langle T_2^2\rangle}}. \tag{86}$$

(Note that due to stationarity, switching T_1 and T_2 in the definition is equivalent to $\tau\to-\tau$.) Selected cross-correlation functions for the Lagrangian time series in Fig. 14 are shown in Fig. 16. In the top-left figure, we see that z^* and ω^* are essentially uncorrelated, as expected. (This would not be the case for non-Gaussian scalars!) In the bottom-left figure, we see that the cross-correlation between ω^* and $\langle\epsilon_\alpha\rangle^*$ is strong, and nearly symmetric with respect to $\tau=0$. The cross-correlation between ω^* and $\langle\epsilon_\beta\rangle^*$ (bottom right), on the other hand, is important only for nonnegative time lags. The same type of behavior is seen with the cross-correlation between $\langle\epsilon_\alpha\rangle^*$ and $\langle\epsilon_\beta\rangle^*$ (top right). As is evident by inspecting the time series themselves in Fig. 14, these results show that $\langle\epsilon_\alpha\rangle^*(t)$ tracks more closely $\omega^*(t)$ than does $\langle\epsilon_\beta\rangle^*(t)$. In future work, we plan to examine how well these predictions match data from DNS Lagrangian time series.

VI. CONCLUSIONS AND FUTURE WORK

Overall, the LSR model yields satisfactory agreement with the DNS data for differential-diffusion effects for Gaussian scalar fields evolving in stationary, isotropic turbulence. Compared to full spectral transport models, the computational requirements for the LSR model are negligible,

making it applicable to more complex flows than those considered here. The model's success at handling differential-diffusion effects can be directly attributed to three key modeling assumptions.

(1) Backscatter, as quantified by the parameter c_d, is responsible for transporting decorrelation generated at small scales by differential diffusion back to large scales.
(2) The steady-state mechanical-to-scalar time-scale ratio depends on the Schmidt number, in general, and through the function $h(\mathrm{Sc})$ in the backscatter rate constant for the diffusive range, in particular.
(3) The characteristic molecular diffusion frequency $\langle r_{\alpha\beta}\rangle_D$ is inversely proportional to the scalar covariance in the dissipative range $\langle \phi'_\alpha \phi'_\beta\rangle_D$ (as opposed to the total covariance $\langle \phi'_\alpha \phi'_\beta\rangle$).

It is important to stress that all three assumptions are required for a successful model. For example, (1) without (2) is not sufficient to cause decorrelation to propagate back to large scales; and (3) is needed to predict the correct decorrelation at small scales, as well as to keep the model well defined when the mean scalar gradients are inverted. Nevertheless, for differential diffusion (2) is perhaps the most critical because it directly determines the long-time scalar decorrelation rate in the absence of mean scalar gradients, and the Sc and Re dependence of the scalar difference variance $\langle z^2\rangle$. For this reason, it is of considerable interest to explore the Sc dependence of β_D using DNS data[11] for spectral transport in isotropic turbulence, and such a study is currently underway.

The LSR model results presented here and in earlier work[21,20] suggest several areas for future research. At the basic level of model formulation, it would be of interest to test the dependence of the model's parameters (e.g., α_{ij}, β_{ij}, c_d, etc.) on the Reynolds number and on the presence of a mean scalar gradient and/or mean shear. This could be done by extracting the forward and backscatter rates from DNS data for homogeneous turbulence.[45] Another line of investigation that appears promising is to use Lagrangian time series from DNS to validate the LSR model predictions of correlation functions like those presented in Figs. 14–16. This information will be particularly important for future applications of the LSR model to turbulent reacting flows. For the latter, it is imperative[44] that appropriate models for molecular mixing be developed and validated. For example, the Fokker–Planck model developed in this work requires information on the forms of the conditional scalar Laplacians $\langle \Gamma_\alpha \nabla^2 \phi'_\alpha | \phi'^*_\alpha, \phi'^*_\beta\rangle$ and the conditional (joint) scalar dissipation rates $\langle \epsilon_{\alpha,\beta} | \phi'^*_\alpha, \phi'^*_\beta\rangle$ for *non-Gaussian scalars*. Although it is unlikely that these functions will be simple, they can be extracted from DNS data for scalar mixing with or without chemical reactions, and perhaps used to suggest simpler approximations that could be employed in the molecular mixing model. Ultimately, we would like to apply the LSR model in full pdf simulations of turbulent reacting flows with local extinction in order to investigate the importance of various physical phenomena (scalar dissipation rate fluctuations, differential diffusion, etc.) on pollutant formation in practical combustion devices. However, as a first step, it would be necessary and enlightening to validate the model's predictions using high-quality DNS data for turbulent scalar mixing with ''model thermochemistry.''[40,44]

ACKNOWLEDGMENTS

This work was supported by the National Science Foundation under Grant No. CTS-9720205 and The Kansas Program for Complex Fluid Flows. The author thanks P. K. Yeung for providing his DNS data prior to publication, and for enlightening discussions on the spectral interpretation of differential diffusion. He also thanks L. Vervisch and his colleagues at CORIA in Rouen, France where this work was initiated for their hospitality and helpful comments.

APPENDIX: RELATIONSHIP BETWEEN THE SR MODEL AND THE SCALAR SPECTRUM EVOLUTION EQUATIONS

In the presence of a mean scalar gradient $\nabla\Phi_\alpha$ and a fluctuating (zero-mean) velocity field u_i, the fluctuation field of a passive scalar ϕ'_α with molecular diffusion coefficient Γ_α is governed by

$$\frac{\partial \phi'_\alpha}{\partial t} + u_i \frac{\partial \phi'_\alpha}{\partial x_i} = -u_i \frac{\partial \Phi_\alpha}{\partial x_i} + \Gamma_\alpha \frac{\partial^2 \phi'_\alpha}{\partial x_i \partial x_i}. \tag{A1}$$

The time-evolution equation for the spherically-integrated scalar-variance spectrum $E_{\alpha\alpha}(\kappa,t)$ obtained from Eq. (A1) can be written as

$$\frac{\partial}{\partial t} E_{\alpha\alpha}(\kappa,t) = G_{\alpha\alpha}(\kappa,t) + T_{\alpha\alpha}(\kappa,t) - 2\frac{\nu}{\mathrm{Sc}_\alpha}\kappa^2 E_{\alpha\alpha}(\kappa,t), \tag{A2}$$

where $\mathrm{Sc}_\alpha = \nu/\Gamma_\alpha$, $G_{\alpha\alpha}$ is the scalar-variance source term proportional to the uniform mean scalar gradient and the scalar-flux spectrum, and $T_{\alpha\alpha}$ is the scalar-variance transfer spectrum.

Likewise, the time-evolution equation for the scalar-covariance spectrum $E_{\alpha\beta}(\kappa,t)$ can be written as

$$\frac{\partial}{\partial t} E_{\alpha\beta}(\kappa,t) = G_{\alpha\beta}(\kappa,t) + T_{\alpha\beta}(\kappa,t) - 2\frac{\nu}{\mathrm{Sc}_{\alpha\beta}}\kappa^2 E_{\alpha\beta}(\kappa,t), \tag{A3}$$

where $\mathrm{Sc}_{\alpha\beta} = 2\nu/(\Gamma_\alpha + \Gamma_\beta)$, $G_{\alpha\beta}$ is the corresponding scalar-covariance source term, and $T_{\alpha\beta}$ is the scalar-covariance transfer spectrum. In the following, we will relate the SR model for the scalar variance to Eq. (A2); however, analogous expressions can be derived for the scalar covariance from Eq. (A3).

A key assumption in deriving the SR model (as well as earlier spectral models[27,46–48]) is that the transfer spectrum is a linear operator with respect to the scalar spectrum (e.g., a linear convection-diffusion model) which has a characteristic time constant that depends only on the velocity spectrum. The linearity assumption [which is consistent with the linear form of Eq. (A1)] ensures not only that the scalar transfer spectra are conservative, but also that if $\mathrm{Sc}_{\alpha\beta} = \mathrm{Sc}_\gamma$ in Eq. (A3), then $E_{\alpha\beta}(\kappa,t) = E_{\gamma\gamma}(\kappa,t)$ for all t when it is true for $t=0$. In the SR model, the linearity assumption implies that the forward and backscatter rate constants (defined below) have the same form for both the variance and covariance

spectra, and that for the covariance spectrum the rate constants depend on the molecular diffusivities only through $\mathrm{Sc}_{\alpha\beta}$ (i.e., not independently on Sc_α or Sc_β).

Following Yeung,[11,25] the transfer spectra can be decomposed into contributions from velocity and scalar modes in specified scale ranges. For example, letting $T_{\alpha\alpha}(\kappa|p,q)$ denote the contribution from the velocity mode centered at p and the scalar mode centered at q, the scalar-variance transfer spectrum can be expressed as

$$T_{\alpha\alpha}(\kappa,t)=\int_0^\infty\int_0^\infty T_{\alpha\alpha}(\kappa|p,q)dpdq=\int_0^\infty S_{\alpha\alpha}(\kappa|q)dq. \tag{A4}$$

The scalar-scalar transfer function $S_{\alpha\alpha}(\kappa|q)$ appearing in the final term on the right-hand side of Eq. (A4) denotes the contribution of scalar mode q to the scalar-variance transfer spectrum at κ. (See Yeung[11,25] for examples of these functions extracted from DNS.) Similarly, the scalar-covariance transfer spectrum can be decomposed using $T_{\alpha\beta}(\kappa|p,q)$ and $S_{\alpha\beta}(\kappa|q)$.

The scalar-scalar transfer function can be used to decompose the scalar-variance transfer spectrum into forward-transfer and backscatter contributions:

$$T_{\alpha\alpha}(\kappa,t)=T^{>}_{\alpha\alpha}(\kappa,t)+T^{<}_{\alpha\alpha}(\kappa,t), \tag{A5}$$

where the forward-transfer contribution is defined by

$$T^{>}_{\alpha\alpha}(\kappa,t)=\int_0^\kappa S_{\alpha\alpha}(\kappa|q)dq, \tag{A6}$$

and the backscatter contribution is defined by

$$T^{<}_{\alpha\alpha}(\kappa,t)=\int_\kappa^\infty S_{\alpha\alpha}(\kappa|q)dq. \tag{A7}$$

Consistent with these definitions, DNS data[11,25] show that $T^{>}_{\alpha\alpha}$ is always positive, while $T^{<}_{\alpha\alpha}$ is always negative. Analogous definitions and remarks hold for the scalar-covariance transfer function, i.e., for $T^{>}_{\alpha\beta}$ and $T^{<}_{\alpha\beta}$.

The scalar coherency spectrum is defined in terms of the variance and covariance spectra by

$$\rho_{\alpha\beta}(\kappa,t)=\frac{E_{\alpha\beta}(\kappa,t)}{\sqrt{E_{\alpha\alpha}(\kappa,t)E_{\beta\beta}(\kappa,t)}}. \tag{A8}$$

(The ''banded'' coherency spectrum has an analogous definition[7] where the energy spectra are replaced with the spectra integrated over a finite wavenumber band.) From the spectral time-evolution equations, it is easily shown that in the absence of mean scalar gradients the time evolution of the coherency spectrum is governed by

$$\frac{1}{\rho_{\alpha\beta}}\frac{\partial\rho_{\alpha\beta}}{\partial t}=\frac{T_{\alpha\beta}}{E_{\alpha\beta}}-\frac{1}{2}\frac{T_{\alpha\alpha}}{E_{\alpha\alpha}}-\frac{1}{2}\frac{T_{\beta\beta}}{E_{\beta\beta}}. \tag{A9}$$

Thus, as noted earlier by Yeung and Pope,[7] since the molecular diffusivities do not appear on the right-hand side, molecular differential diffusion affects the coherency only indirectly, i.e., through interscale transfer processes which propagate incoherency from small scales to large scales. The choice of the model for the scalar transfer spectra thus completely determines the long-time behavior of $\rho_{\alpha\beta}$ in the absence of mean scalar gradients.

The SR model can be related to Eq. (A2), starting from Eq. (16) and using the cut-off wavenumbers κ_0, κ_{2j}, and κ_D. For example, integrating Eq. (A2) over the wavenumber band $[\kappa_D,\infty)$ yields the exact time-evolution equation for $\langle\phi'^2_\alpha\rangle_D$:

$$\frac{d\langle\phi'^2_\alpha\rangle_D}{dt}=2\gamma_D S_\alpha+2T_D-2\langle\epsilon_\alpha\rangle_D. \tag{A10}$$

The right-hand side of this expression is defined in terms of $G_{\alpha\alpha}$, $S_{\alpha\alpha}(\kappa|q)$, and $\Gamma_\alpha\kappa^2E_{\alpha\alpha}$ as discussed next. Similar expressions can be derived for the other variables in the SR model by integrating Eq. (A2) over the corresponding wavenumber bands.

The scalar-variance source term in Eq. (A10) is defined by

$$S_\alpha=\frac{1}{2}\int_0^\infty G_{\alpha\alpha}(\kappa,t)d\kappa, \tag{A11}$$

and the fraction of the scalar-variance source term falling in the final wavenumber band is defined by

$$\gamma_D=\frac{1}{2S_\alpha}\int_{\kappa_D}^\infty G_{\alpha\alpha}(\kappa,t)d\kappa. \tag{A12}$$

In the present version of the SR model, the fractions γ_{ij} are assumed to be time-independent functions of Re_1 and Sc. Likewise, the scalar-variance source term is modeled by a gradient-diffusion closure [Eq. (9)]. The SR model could thus be further refined (with increased computational expense) by including an explicit model for the scalar-flux spectrum.

The scalar dissipation term in Eq. (A10) is defined by

$$\langle\epsilon_\alpha\rangle_D=\int_{\kappa_D}^\infty\Gamma_\alpha\kappa^2E_{\alpha\alpha}(\kappa,t)d\kappa. \tag{A13}$$

In the SR model, κ_D is chosen such that $\langle\epsilon_\alpha\rangle_D\approx\langle\epsilon_\alpha\rangle$, i.e., so that the bulk of the scalar dissipation occurs in the final wavenumber band. Thus, the scalar dissipation terms appearing in other wavenumber bands are assumed to be negligible. Note that, unlike with the continuous representation [Eq. (A2)], the discrete representation used in the SR model requires an explicit model for the scalar dissipation rate $\langle\epsilon_\alpha\rangle$.

The spectral transport term in Eq. (A10) is defined by

$$T_D(t)=\frac{1}{2}\int_{\kappa_D}^\infty T^{>}_{\alpha\alpha}(\kappa,t)d\kappa+\frac{1}{2}\int_{\kappa_D}^\infty T^{<}_{\alpha\alpha}(\kappa,t)d\kappa. \tag{A14}$$

In the SR model, forward and backscatter rate constants are employed to model the spectral transport terms. These rate constants can be expressed explicitly in terms of the scalar-variance transfer spectrum decomposed into forward and backscatter contributions. For example,

$$\alpha_{2\,n_2}=\frac{1}{2\langle\phi'^2_\alpha\rangle_{2\,n_2}}\int_{\kappa_D}^\infty T^{>}_{\alpha\alpha}(\kappa,t)d\kappa \tag{A15}$$

and

$$\beta_D = -\frac{1}{2\langle \phi_\alpha'^2 \rangle_D} \int_{\kappa_D}^{\infty} T_{\alpha\alpha}^{<}(\kappa,t)\, d\kappa. \tag{A16}$$

Note that the right-hand sides of these expressions can be extracted from DNS data for homogeneous turbulence in order to explore the dependence of the rate constants on Re_1 and Sc. Results from a preliminary investigation for $R_\lambda = 90$ have revealed that the backscatter rate constant from the dissipative range can be closely approximated by $\beta_D \sim \mathrm{Sc}^{1/2} \sim \kappa_D/\kappa_\eta$ for Sc in the range [1/8,1]. (More extensive results will be reported in a future communication.) On the other hand, for cut-off wavenumbers in the inertial-convective subrange, one would expect α_{2j} and β_{2j} to be independent of Sc. This is the assumption employed in the SR model, but it can be validated (and modified) using DNS data for the scalar spectrum and the scalar–scalar transfer function. The linearity assumption discussed earlier implies that the rate constants will be unchanged (for the same Reynolds and Schmidt numbers) when they are computed using the scalar-covariance transfer spectrum.

Note that at spectral equilibrium the integral in Eq. (A15) will be constant and proportional to $\langle \epsilon_\alpha \rangle$ (i.e., the scalar spectral energy transfer rate in the inertial-convective subrange will be constant). The forward rate constants α_{2j} will thus depend on the chosen cut-off wavenumbers through their effect on $\langle \phi_\alpha'^2 \rangle_{2j}$. In the SR model, in order to obtain the most computationally-efficient spectral model possible, the total number of wavenumber bands is minimized subject to the condition that

$$\frac{\langle \epsilon \rangle}{k} \leqslant \alpha_1 \leqslant \alpha_{21} \leqslant \cdots \leqslant \alpha_{2\,n_2}. \tag{A17}$$

Assuming a fully-developed $(-5/3)$ velocity spectrum, this process results[20,21] in the cut-off wavenumbers given in Eq. (19). An obvious extension of the model would thus be to include a dynamical model for the velocity spectrum.[49,50] However, including a more detailed model for the turbulence/scalar-flux spectra would most likely make the extension to a Lagrangian PDF formulation computationally intractable for practical reacting flow calculations.

The final expression needed to complete the SR model is a closure for $\langle \epsilon_\alpha \rangle_D$ appearing in Eq. (A10). In order to develop a model starting from Eq. (A2), we will first introduce the scalar dissipation spectrum defined by $D_{\alpha\alpha} = \Gamma_\alpha \kappa^2 E_{\alpha\alpha}$, the scalar spectral energy transfer rate $\mathcal{T}_{\alpha\alpha}$, defined by

$$\mathcal{T}_{\alpha\alpha}(\kappa,t) = \int_{\kappa}^{\infty} T_{\alpha\alpha}(s,t)\, ds, \tag{A18}$$

and a characteristic spectral time scale τ_{st} defined by

$$\tau_{st}(\kappa,t) = \frac{\kappa E_{\alpha\alpha}(\kappa,t)}{\mathcal{T}_{\alpha\alpha}(\kappa,t)}. \tag{A19}$$

Note that in the viscous subrange,[27,18] τ_{st} is proportional to $(\nu/\langle \epsilon \rangle)^{1/2}$.

Multiplication of Eq. (A2) by $\Gamma_\alpha \kappa^2$, and integration of the resultant expression over the wavenumber range $[\kappa_D, \infty)$ using Eqs. (A18) and (A19), yields

$$\frac{d\langle \epsilon_\alpha \rangle_D}{dt} = \int_{\kappa_D}^{\infty} \Gamma_\alpha \kappa^2 G_{\alpha\alpha}(\kappa,t)\, d\kappa + \Gamma_\alpha \kappa_D^2 \mathcal{T}_{\alpha\alpha}(\kappa_D,t) + 2\int_{\kappa_D}^{\infty} \frac{D_{\alpha\alpha}(\kappa,t)}{\tau_{st}(\kappa,t)}\, d\kappa - \mathcal{D}_{\alpha\alpha}, \tag{A20}$$

where the dissipation term $\mathcal{D}_{\alpha\alpha}$ is defined by

$$\mathcal{D}_{\alpha\alpha} = 2\int_{\kappa_D}^{\infty} \Gamma_\alpha \kappa^2 D_{\alpha\alpha}(\kappa,t)\, d\kappa. \tag{A21}$$

The right-hand side of Eq. (A20) contains unclosed terms that must be modeled in order to arrive at Eq. (28). This process is explained next.

The first term on the right-hand side of Eq. (A20) is a source term due to the mean scalar gradient. In Eq. (28), the following model is employed:

$$\frac{\langle \epsilon_\alpha \rangle_D}{\langle \phi_\alpha'^2 \rangle_D} = \frac{\int_{\kappa_D}^{\infty} \Gamma_\alpha \kappa^2 G_{\alpha\alpha}(\kappa,t)\, d\kappa}{\int_{\kappa_D}^{\infty} G_{\alpha\alpha}(\kappa,t)\, d\kappa}. \tag{A22}$$

Note that this model is exact if $G_{\alpha\alpha} \propto E_{\alpha\alpha}$ in the scalar-dissipation range.

The second term on the right-hand side of Eq. (A20) represents the flux of scalar dissipation into the scalar-dissipation range, and can be rewritten in terms of known quantities. From Eq. (A18), it can be seen that $\mathcal{T}_{\alpha\alpha}(\kappa_D,t) = 2T_D(t)$. Likewise, using the definition of κ_D, it follows that $\Gamma_\alpha \kappa_D^2 = C_D(\langle \epsilon \rangle/\nu)^{1/2}$. The scalar-dissipation flux term can thus be expressed as

$$2C_D\left(\frac{\langle \epsilon \rangle}{\nu}\right)^{1/2} T_D(t) = 2C_D\left(\frac{\langle \epsilon \rangle}{\nu}\right)^{1/2} \alpha_{2\,n_2} \langle \phi_\alpha'^2 \rangle_{2n_2} - 2C_D\left(\frac{\langle \epsilon \rangle}{\nu}\right)^{1/2} \beta_D \langle \phi_\alpha'^2 \rangle_D. \tag{A23}$$

However, to ensure that the model is numerically stable, the last term on the right-hand side of this expression is replaced with its spectral equilibrium value: $-2\beta_D \langle \epsilon_\alpha \rangle_D$.

The next term in Eq. (A20) is modeled by assuming that $\tau_{st}(\kappa,t) \sim (\nu/\langle \epsilon \rangle)^{1/2}$ for all wavenumbers in the range $[\kappa_D, \infty)$. The validity of this assumption depends on the Schmidt number, but it is strictly valid for $1 \leqslant \mathrm{Sc}$. Using this assumption, we can extract τ_{st} from the integral in the second term on the right-hand side of Eq. (A20) so that the entire term becomes $2C_s(\langle \epsilon \rangle/\nu)^{1/2} \langle \epsilon_\alpha \rangle_D$. The proportionality constant can be split into two contributions: $C_s = C_B - C_D$, where

$$C_B = \frac{1}{2\langle \epsilon_\alpha \rangle_D} \left(\frac{\nu}{\langle \epsilon \rangle}\right)^{1/2} \int_{\kappa_D}^{\infty} \Gamma_\alpha \kappa^2 T_{\alpha\alpha}(\kappa,t)\, d\kappa. \tag{A24}$$

In the SR model, $C_s = 1/2$ which can validated using DNS data. Note that at spectral equilibrium $T_D \sim \langle \epsilon_\alpha \rangle$ so that the first two terms on the right-hand side of Eq. (A20) function as a linear source term of the form $2C_B(\langle \epsilon \rangle/\nu)^{1/2} \langle \epsilon_\alpha \rangle_D$.

The final term in Eq. (A20) ($\mathcal{D}_{\alpha\alpha}$) is modeled by the product of the inverse of a characteristic time scale for the scalar dissipation range and $\langle \epsilon_\alpha \rangle_D$. The characteristic time

scale is taken to be proportional to $\langle \phi_\alpha'^2 \rangle_D / \langle \epsilon_\alpha \rangle_D$ so that the final term has the form $2C_d \langle \epsilon_\alpha \rangle_D^2 / \langle \phi_\alpha'^2 \rangle_D$. The proportionality constant C_d is thus defined by

$$C_d = \frac{\langle \phi_\alpha'^2 \rangle_D}{\langle \epsilon_\alpha \rangle_D^2} \int_{\kappa_D}^{\infty} \Gamma_\alpha^2 \kappa^4 E_{\alpha\alpha}(\kappa, t) d\kappa. \tag{A25}$$

In the SR model, $C_d = 3$ is chosen to agree with passive scalar decay from isotropic initial conditions in the absence of turbulent mixing (i.e., pure diffusion).

At spectral equilibrium, the dissipation term will be in dynamic equilibrium with the linear source term. Moreover, the scalar dissipation rate will be controlled by the cascade of scalar energy into the inertial-convective subrange. From the SR model, we then find $\langle \epsilon_\alpha \rangle \propto \mathrm{Sc}^{-s} \langle \omega \rangle \langle \phi_\alpha'^2 \rangle$. Ignoring the source term due to the mean scalar gradient (i.e., at high Reynolds numbers), Eq. (A20) reduces at spectral equilibrium to

$$0 = 2C_B (\langle \epsilon \rangle / \nu)^{1/2} \langle \epsilon_\alpha \rangle_D - 2C_d \frac{\langle \epsilon_\alpha \rangle_D}{\langle \phi_\alpha'^2 \rangle_D} \langle \epsilon_\alpha \rangle_D. \tag{A26}$$

From this expression, the equilibrium fraction of the scalar spectrum in the dissipative range is found to be

$$\gamma_D = \frac{\langle \epsilon_\alpha \rangle_D}{\langle \epsilon_\alpha \rangle} \frac{C_d}{C_B} \frac{1}{\mathrm{Re}_1}. \tag{A27}$$

Starting from Eq. (A3), analogous arguments/assumptions as those leading to the model for $\langle \epsilon_\alpha \rangle$ can be used to derive the SR model equation for $\langle \epsilon_{\alpha\beta} \rangle$. Note that DNS data for passive scalar mixing in homogeneous turbulence can be employed to validate all SR model constants, and to explore possible dependencies on Re_1 and Sc (e.g., due to low-Reynolds number effects). Results from such a study will be reported in a future communication.

[1] R. W. Bilger, ''Molecular transport effects in turbulent diffusion flames at moderate Reynolds number,'' AIAA J. **20**, 962 (1982).
[2] R. W. Bilger and R. W. Dibble, ''Differential molecular diffusion effects in turbulent mixing,'' Combust. Sci. Technol. **28**, 161 (1982).
[3] S. B. Pope, ''Computations of turbulent combustion: progress and challenges,'' *23rd Symposium (International) on Combustion*, The Combustion Institute, 1990, p. 591.
[4] M. C. Drake, R. W. Pitz, and M. Lapp, ''Laser measurements on nonpremixed H_2-air flames for assessments of turbulent combustion models,'' AIAA J. **24**, 905 (1986).
[5] L. L. Smith, R. W. Dibble, L. Talbot, R. S. Barlow, and C. D. Carter, ''Laser Raman scattering measurements of differential molecular diffusion in non-reacting turbulent jets of H_2/CO_2 mixing with air,'' Phys. Fluids **7**, 1455 (1995).
[6] J. R. Saylor and K. R. Sreenivasan, ''Differential diffusion in low Reynolds number water jets,'' Phys. Fluids **10**, 1135 (1998).
[7] P. K. Yeung and S. B. Pope, ''Differential diffusion of passive scalars in isotropic turbulence,'' Phys. Fluids A **5**, 2467 (1993).
[8] P. K. Yeung and B. Luo, ''Simulation and modeling of differential diffusion in homogeneous turbulence,'' *Proceedings of the 10th Symposium on Turbulent Shear Flows*, University Park, PA, 1995, pp. 31–37.
[9] P. K. Yeung and C. A. Moseley, ''Effects of mean scalar gradients on differential diffusion in isotropic turbulence,'' AIAA Paper 95-0866, 1995.
[10] A. Juneja and S. B. Pope, ''A DNS study of turbulent mixing of two passive scalars,'' Phys. Fluids **8**, 2161 (1996).
[11] P. K. Yeung, ''Multi-scalar triadic interactions in differential diffusion with and without mean scalar gradients,'' J. Fluid Mech. **321**, 235 (1996).
[12] A. Kronenburg and R. W. Bilger, ''Modeling of differential diffusion effects in nonpremixed nonreacting turbulent flow,'' Phys. Fluids **9**, 1435 (1997).
[13] V. Nilsen and G. Kosály, ''Differentially diffusing scalars in turbulence,'' Phys. Fluids **9**, 3386 (1997).
[14] V. Nilsen and G. Kosály, ''Differential diffusion in turbulent reacting flows,'' Combust. Flame **117**, 493 (1999).
[15] P. K. Yeung, ''Correlations and conditional statistics in differential diffusion: Scalars with uniform mean gradients,'' Phys. Fluids **10**, 2621 (1998).
[16] A. R. Kerstein, ''Linear-eddy modelling of turbulent transport. Part 3. Mixing and differential diffusion in round jets,'' J. Fluid Mech. **216**, 411 (1990).
[17] A. R. Kerstein, M. A. Cremer, and P. A. McMurtry, ''Scaling properties of differential molecular effects in turbulence,'' Phys. Fluids **7**, 1999 (1995).
[18] J. R. Chasnov, ''The viscous-convective subrange in nonstationary turbulence,'' Phys. Fluids **10**, 1191 (1998).
[19] R. O. Fox, ''Computational methods for turbulent reacting flows in the chemical process industry,'' Rev. Inst. Français d Pétrole **51**, 215 (1996).
[20] R. O. Fox, ''The Lagrangian spectral relaxation model of the scalar dissipation in homogeneous turbulence,'' Phys. Fluids **9**, 2364 (1997).
[21] R. O. Fox, ''The spectral relaxation model of the scalar dissipation rate in homogeneous turbulence,'' Phys. Fluids **7**, 1082 (1995).
[22] R. O. Fox, ''The Fokker–Planck closure for turbulent molecular mixing: Passive scalars,'' Phys. Fluids A **4**, 1230 (1992).
[23] R. O. Fox, ''Improved Fokker–Planck model for the joint scalar, scalar gradient pdf,'' Phys. Fluids **6**, 334 (1994).
[24] C. W. Gardiner, *Handbook of Stochastic Methods*, 2nd ed. (Springer-Verlag, New York, 1990).
[25] P. K. Yeung, ''Spectral transport of self-similar passive scalar fields in isotropic turbulence,'' Phys. Fluids **6**, 2245 (1994).
[26] P. K. Yeung (private communication), 1998.
[27] G. K. Batchelor, ''Small-scale variation of convected quantities like temperature in a turbulent field. Part 1. General discussion and the case of small conductivity,'' J. Fluid Mech. **5**, 113 (1959).
[28] J. P. H. Sanders and I. Gökalp, ''Scalar dissipation rate modelling in variable density turbulent axisymmetric jets and diffusion flames,'' Phys. Fluids **10**, 938 (1998).
[29] S. B. Pope and Y. L. Chen, ''The velocity-dissipation probability density function model for turbulent flows,'' Phys. Fluids A **2**, 1437 (1990).
[30] S. B. Pope, ''Application of the velocity-dissipation probability density function model to inhomogeneous turbulent flows,'' Phys. Fluids A **3**, 1947 (1991).
[31] M. R. Overholt and S. B. Pope, ''DNS of a passive scalar with imposed mean gradient in isotropic turbulence,'' Phys. Fluids **8**, 3128 (1996).
[32] T. D. Dreeben and S. B. Pope, ''Wall-function treatment in pdf methods for turbulent flows,'' Phys. Fluids **9**, 2692 (1997).
[33] L. Valino, C. Dopazo, and J. Ros, ''Quasistationary probability density functions in the turbulent mixing of a scalar field,'' Phys. Rev. Lett. **72**, 3518 (1993).
[34] S. B. Pope and E. S. C. Ching, ''The stationary probability density function: An exact result,'' Phys. Fluids A **5**, 1529 (1993).
[35] A. Sahay and E. E. O'Brien, ''Uniform mean scalar gradient in grid turbulence: Conditional dissipation and production,'' Phys. Fluids A **5**, 1076 (1993).
[36] X. D. Cai, E. E. O'Brien, and F. Ladiende, ''Uniform mean scalar gradient in grid turbulence: Asymptotic probability distribution of a passive scalar,'' Phys. Fluids **8**, 2555 (1996).
[37] V. A. Sabel'nikov, ''Asymptotic solution of the equation for the probability distribution of a passive scalar in grid turbulence with a uniform mean scalar gradient,'' Phys. Fluids **10**, 753 (1998).
[38] S. B. Pope, ''Lagrangian pdf methods for turbulent flows,'' Annu. Rev. Fluid Mech. **26**, 23 (1993).
[39] P. E. Kloeden and E. Platen, *Numerical Solution of Stochastic Differential Equations* (Springer, Verlag, New York, 1992).
[40] Y. Y. Lee and S. B. Pope, ''Nonpremixed turbulent reacting flow near extinction,'' Combust. Flame **101**, 501 (1995).
[41] S. Mahalingam, J. H. Chen, and L. Vervisch, ''Finite-rate chemistry and transient effects in direct numerical simulations of turbulent nonpremixed flames,'' Combust. Flame **102**, 285 (1995).
[42] C. J. Montgomery, G. Kosály, and J. J. Riley, ''Direct numerical simulation of turbulent nonpremixed combustion with multistep hydrogen-oxygen kinetics,'' Combust. Flame **109**, 113 (1997).
[43] N. Swaminathan and R. W. Bilger, ''Direct numerical simulation of turbulent nonpremixed hydrocarbon reaction zones using a two-step reduced

mechanism,'' Combust. Sci. Technol. **127**, 167 (1997).
[44]M. R. Overholt and S. B. Pope, ''Numerical Investigation of a statistically stationary turbulent reacting flow,'' Combust. Theory Modelling (in press).
[45]P. K. Yeung and Y. Zhou, ''Analysis of subgrid eddy diffusivity in turbulence using direct numerical simulation databases,'' AIAA Paper No. 96-3074, 1996.
[46]P. G. Saffman, ''On the fine-scale structure of vector fields convected by a turbulent field,'' J. Fluid Mech. **16**, 545 (1963).
[47]R. H. Kraichnan, ''Small-scale structure of a scalar field convected by turbulence,'' Phys. Fluids **11**, 945 (1968).
[48]R. H. Kraichnan, ''Convection of a passive scalar by a quasi-uniform random straining field,'' J. Fluid Mech. **64**, 737 (1974).
[49]T. T. Clark and C. Zemach, ''A spectral model applied to homogeneous turbulence,'' Phys. Fluids **7**, 1674 (1995).
[50]V. M. Canuto and M. S. Dubovikov, ''A dynamical model for turbulence. I. General formalism,'' Phys. Fluids **8**, 571 (1996).